# APLF and long non-coding RNA NIHCOLE promote stable DNA synapsis in non-homologous end joining

Cell Reports

Article

# APLF and long non-coding RNA NIHCOLE promote stable DNA synapsis in non-homologous end joining

## Graphical abstract

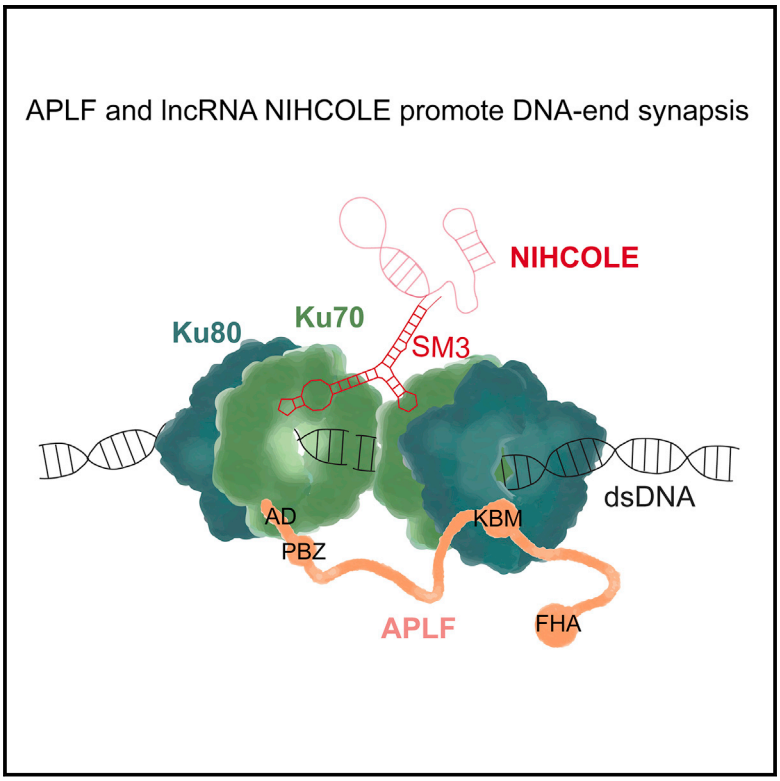


## Authors

Sara De Bragança, Clara Aicart-Ramos, Raquel Arribas-Bosacoma, ..., Puri Fortes, Oscar Llorca, Fernando Moreno-Herrero

## Correspondence

ollorca@cnio.es (O.L.), fernando.moreno@cnb.csic.es (F.M.-H.)

## In brief

DNA repair via non-homologous end joining is regulated by poorly understood accessory factors. De Bragança et al. find that APLF promotes the stable joining of DNA ends by Ku70-Ku80, further reinforced by long non-coding RNA NIHCOLE. They propose that Ku70-Ku80 simultaneously binds DNA ends, APLF, and lncRNAs to strengthen DNA synapsis.

## Highlights

- In NHEJ, APLF promotes synapsis of DNA ends for several minutes under piconewton forces
- Ku70-Ku80 and APLF establish a minimal complex sufficient to support DNA synapsis
- Long non-coding RNA NIHCOLE stabilizes a DNA synapsis mediated by Ku70-Ku80 and APLF
- A small and structured RNA domain of NIHCOLE promotes stable joining of DNA ends

De Bragança et al., 2023, Cell Reports *42*, 111917
January 31, 2023 
https://doi.org/10.1016/j.celrep.2022.111917

CellPress

Cell Reports

CellPress
OPEN ACCESS

Article

# APLF and long non-coding RNA NIHCOLE promote stable DNA synapsis in non-homologous end joining

Sara De Bragança,[1] Clara Aicart-Ramos,[1] Raquel Arribas-Bosacoma,[2] Angel Rivera-Calzada,[3] Juan Pablo Unfried,[4,5] Laura Prats-Mari,[5] Mikel Marin-Baquero,[1] Puri Fortes,[5,6,7] Oscar Llorca,[3,*] and Fernando Moreno-Herrero[1,8,*]

[1]Department of Macromolecular Structures, Centro Nacional de Biotecnología (CNB), CSIC, Madrid, Spain
[2]Genome Damage and Stability Centre, School of Life Sciences, University of Sussex, Brighton, UK
[3]Structural Biology Programme, Spanish National Cancer Research Center (CNIO), Madrid, Spain
[4]Department of Biological Regulation, Weizmann Institute of Science, Rehovot, Israel
[5]Department of Gene Therapy and Regulation of Gene Expression, Center for Applied Medical Research (CIMA), University of Navarra (UNAV), Pamplona, Spain
[6]Navarra Institute for Health Research (IdiSNA), Pamplona, Spain
[7]Liver and Digestive Diseases Networking Biomedical Research Centre (CIBERehd), Spanish Network for Advanced Therapies (TERAV ISCIII), Madrid, Spain
[8]Lead contact
*Correspondence: ollorca@cnio.es (O.L.), fernando.moreno@cnb.csic.es (F.M.-H.)
https://doi.org/10.1016/j.celrep.2022.111917

## SUMMARY

The synapsis of DNA ends is a critical step for the repair of double-strand breaks by non-homologous end joining (NHEJ). This is performed by a multicomponent protein complex assembled around Ku70-Ku80 heterodimers and regulated by accessory factors, including long non-coding RNAs, through poorly understood mechanisms. Here, we use magnetic tweezers to investigate the contributions of core NHEJ proteins and APLF and lncRNA NIHCOLE to DNA synapsis. APLF stabilizes DNA end bridging and, together with Ku70-Ku80, establishes a minimal complex that supports DNA synapsis for several minutes under piconewton forces. We find the C-terminal acidic region of APLF to be critical for bridging. NIHCOLE increases the dwell time of the synapses by Ku70-Ku80 and APLF. This effect is further enhanced by a small and structured RNA domain within NIHCOLE. We propose a model where Ku70-Ku80 can simultaneously bind DNA, APLF, and structured RNAs to promote the stable joining of DNA ends.

## INTRODUCTION

DNA double-strand breaks (DSBs) are common lesions of the DNA arising from normal cell metabolism or by exposure to ionizing radiation and many chemotherapeutic drugs.[1] The fast repair of DSBs is critical for genome stability and it is tightly regulated. In human cells, there are two main pathways responsible for DSB repair, homologous recombination (HR) and non-homologous end joining (NHEJ).[2,3] While HR requires a template to repair the damaged DNA, NHEJ requires end-proximity for direct repair.[2–4]

NHEJ involves a set of core factors that are sufficient for recognition and ligation of a large fraction of DSBs: the ring-shaped heterodimer formed by Ku70 and Ku80 (Ku70-Ku80, simply stated as Ku hereafter),[5] the XRCC4 (X4)-DNA Ligase IV (LIG4) complex,[6,7] and XLF.[8–10] Ku recognizes the exposed dsDNA ends and threads onto them,[5] offering protection and initiating the recruitment of the other core components to the DSB site. XLF interacts with X4 and contributes to the synapsis between DNA ends.[11–13] The X4-LIG4 complex is responsible for the final step of NHEJ, catalyzing the covalent ligation of the DNA ends.

The catalytic subunit of the DNA-dependent protein kinase (DNA-PKcs) is a relatively recent evolutionary addition to NHEJ present only in vertebrates. In the presence of dsDNA ends, it forms a complex with Ku and it can recruit accessory factors to the break, such as the Artemis endonuclease, which participates in DNA end processing,[14,15] where it also contributes to bringing the two ends of the DNA break in close proximity.[11,12]

DNA end bridging, also called synapsis, is one of the critical events in NHEJ, but the bridging mechanisms have not yet been completely elucidated and several models have been proposed. Using single-molecule experiments and egg extracts from *Xenopus laevis*, Graham et al.[16] proposed that the bridging step occurs in two sub-steps: first, a flexible long-range (LR) bridging interaction is formed that, upon structural remodeling of the synaptic complex, leads to a short-range (SR) conformation in which the DNA ends are sufficiently close to be ligated.[11,16] The structural basis for this transition from long- to SR synapsis has been described. The model suggests that DNA-PKcs is only present in the LR synaptic complex,[11–13] where it helps to tether the DNA ends while supporting the action of end-processing factors that prepare the DNA ends for the next steps of repair.[14] X4 and XLF have a structural role in NHEJ synapsis. They assemble as homodimers and share structural similarities as both present a globular head domain, an

elongated α-helical stalk, and an unstructured C-terminal region.[11,17] Recent structures of short- and LR synaptic complexes show that one XLF dimer interacts with two X4-LIG4 and Ku subcomplexes, each bound to one of the DNA ends, thus supporting the bridging.[11,12] In addition, the C-terminal tail of XLF contains a Ku binding motif (X-KBM) that anchors XLF to Ku-DNA and the intrinsic flexibility of this tail might allow XLF to scan the synaptic complex for interactions.[11,12,18] X4 also plays a role in the stabilization of LIG4, by forming a constitutive complex through a direct interaction mediated by its N-terminal coiled-coil stalk.[6]

In contrast, other authors have found, using super-resolution microscopy in human cells and single-molecule FRET, that DNA-PKcs does not add further efficiency to the DNA end synapsis accomplished by Ku, X4-LIG4, and XLF.[19–22] This suggests that these four proteins are sufficient for synapsis in all eukaryotes.[19,20] Instead, X4 and XLF form extended filaments *in vitro*[23,24] and in cells,[19] and it was proposed that these filament-forming proteins might be sufficient for bridging DNA DSBs *in vivo* in a DNA-PKcs-independent manner.[19] According to this model, after Ku binds to the break, recruitment of X4-LIG4 and XLF would allow the formation of filaments around the two sides of the break that interact and ensure that the DNA ends stay together.[19]

In addition to the core protein factors, the NHEJ pathway comprises end-processing factors, including kinase/phosphatases, nucleases, and polymerases, that chemically modify the damaged DNA ends for ligation, and accessory factors that interact with the core factors of the pathway but whose loss has apparently low impact on NHEJ efficiency.[3] One so-called accessory protein is the Aprataxin-and-PNK-like factor (APLF), whose contribution to the synaptic complex remains unclear. APLF has an intrinsically disordered structure,[25] and although it was first assigned nuclease activity[26–29] it is now believed that it might function as a scaffolding protein[25] recruiting X4-LIG4 and XLF to Ku-bound DNA ends.[30] APLF's N-terminal forkhead-associated (FHA) domain interacts with phosphorylated X4,[26,28,29] while its MID domain contains a 12-amino-acid-long region, known as the APLF Ku-binding motif (A-KBM), which interacts with Ku80, anchoring APLF to DNA-bound Ku.[18,30] APLF also interacts with poly(ADP-ribose) (PAR) via two PAR-binding zinc finger (PBZ) domains[31,32] and binds histones through its C-terminal disordered acidic region.[33,34] APLF facilitates NHEJ, at least in part, by promoting the formation and/or the stability of complexes between Ku and X4-LIG4 on the DNA, which are required for an efficient ligation.[25]

Besides protein factors, accumulating evidence shows that some long non-coding RNAs (lncRNAs) regulate DNA damage response pathways.[35–38] We have reported that lncRNA NIHCOLE enhances DNA ligation efficiency by the NHEJ machinery.[38] NIHCOLE can interact with Ku *in vitro* and in cultured cells. These interactions are relevant in hepatocellular carcinoma, where NIHCOLE is overexpressed and associated with bad prognosis and decreased survival. Other lncRNAs, such as LINP1, LRIK, and recently scaRNA2, have also been assigned an effect in the NHEJ pathway.[35–37] Understanding the mechanism through which lncRNAs influence NHEJ is an active area of current research.

Here, we study the contributions of factors APLF and lncRNA NIHCOLE by implementing a magnetic tweezer (MT) assay to characterize the molecular interactions between DNA ends. This assay allows the direct measurement of the most stable synapses under pulling forces as a readout of the stability and dynamics of the DNA end-bridging process. We found that APLF is critical in establishing stable DNA end synapses in the presence of Ku. In addition, the stability and strength of the synapses notably increased in the presence of lncRNA NIHCOLE, and in particular through the interaction with a small structural domain. These data strongly suggest that the co-occurrence of DNA and RNA binding by Ku plays a role in promoting NHEJ. Collectively, our results suggest that accessory factors APLF and NIHCOLE contribute to NHEJ by stabilizing DNA end bridging in cooperation with Ku70-Ku80.

## RESULTS

### APLF and Ku bridge blunt DNA ends

The contribution of the different NHEJ core factors to the repair of damaged DNA has been traditionally evaluated as a function of ligation efficiency.[30,38,39] Pioneer approaches at the single-molecule level were valuable to identify DNA repair intermediates and to highlight the dynamic interactions in the progression of DNA repair.[19] However, to dissect the synapsis mechanism there is a need for a ligation-independent assay that enables the study of the individual and combined contributions of the different factors involved. To address this, we implemented a single-molecule assay using MTs based on the one introduced by Wang et al.[40] In this assay, a DNA molecule containing two free DNA ends is iteratively extended and relaxed, enabling the bridging of the DNA ends by protein complexes in solution (Figures 1A and 1B). Here, we used a branched DNA construct formed by a central dsDNA fragment of 4.3 kbp with two centric 60-bp-long branches separated from each other by 689 bp (Figure S1A). The DNA constructs were attached to a superparamagnetic bead and immobilized onto a glass surface. A distance-dependent force was applied to the DNA molecules by moving a pair of magnets close to the glass surface. At a 2-pN force, the DNA molecules were extended (Figure 1A, extended [E]), whereas at 0.1 pN the molecules were relaxed, allowing their branches to get close enough to be bridged by NHEJ complexes in solution (Figure 1A, relaxed [R]). When the branches were joined in an end-to-end contact, the apparent extension of the molecule was reduced by 569 bp (Figures 1A, synaptic [S], and S1A). In our assay, the perfectly aligned contact of the ends translated into an experimental reduction of $\Delta z = -0.21 \pm 0.02$ μm, as assessed by a control DNA ends ligation assay using T4 DNA ligase (Figures S1B and S1C). It is important to note that bridging mediated by a protein complex intercalated between the DNA ends would result in extension reductions slightly shifted to less-negative values. The branches of our constructs were blunt with dephosphorylated 5′ ends, preventing covalent ligation and thus allowing us to address DNA end bridging in more detail.

We first confirmed the interactions of Ku with several purified NHEJ factors (Figure S2) in bulk (Figure S3). Ku formed complexes with X4-LIG4 and APLF on DNA in electrophoretic

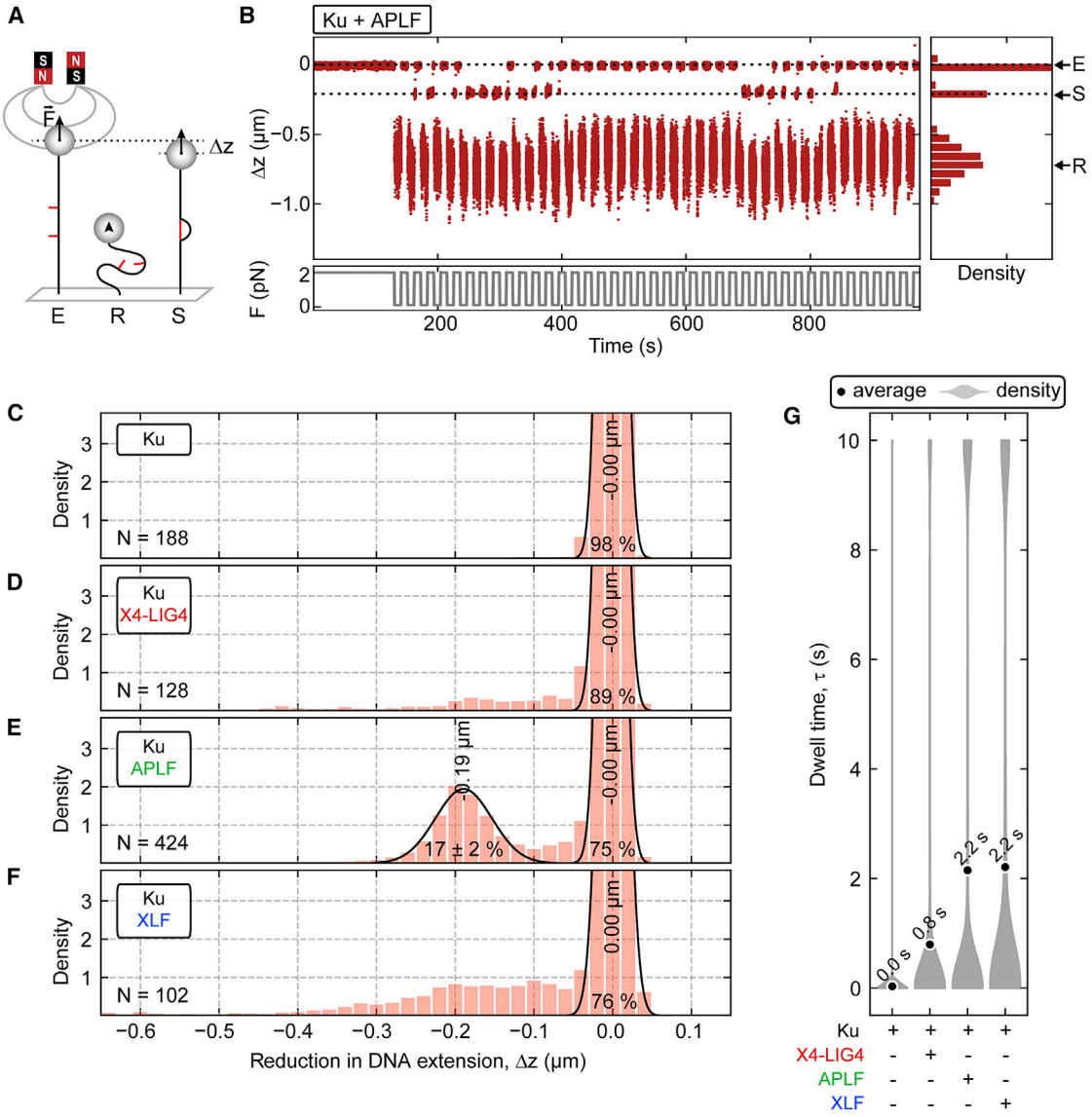


**Figure 1. APLF and Ku bridge blunt DNA ends**

(A) Schematic representation of the magnetic tweezers assay performed on a branched molecule containing two centric DNA ends (see main text for details).

(B) Individual time course of a branched molecule iteratively pulled in the presence of APLF and Ku.

(C–F) Relative reduction distributions for branched DNA molecules in the presence of Ku alone (N = 188), Ku with X4-LIG4 (N = 128), Ku with APLF (N = 424), and Ku with XLF (N = 102), respectively.

(G) Violin plot of the dwell time (τ) distribution for c-f conditions.

mobility shift assays (EMSAs) (Figures S3A and S3B), thereby demonstrating its capacity to reconstitute the interactions already described.[30] X4-LIG4 was active in DNA ligation assays and APLF-enhanced ligation efficiency, as described previously[30] (Figure S3C). Ku also interacted with APLF in the presence of a structural motif from NIHCOLE (Figure S3D), reproducing our previous results.[38] Next, we investigated the bridging capacity of human Ku at the single-molecule level. The branched-DNA construct was immobilized in an MT setup and 1 nM Ku was injected into the chamber. Following an incubation of 5 min, we applied 40 cycles of 10 s at 0.1 pN (relaxation) and 10 s at 2 pN (extension). The relative reductions in DNA extension (Δz) were processed to obtain a normalized distribution that represents the probability of finding a DNA molecule at specific positions). For 1 nM Ku, a single peak at Δz = 0 μm was observed. The peak was fitted to a Gaussian function, leading to a 98% probability of the molecules being extended (Figure 1C). A control experiment without protein showed a relative reduction distribution identical to the one obtained for 1 nM Ku (Figure S4A). In our assay, at 1 nM concentration, Ku was not able to join DNA ends, in accordance with previous works.[20,40] Notably, we observed interactions of Ku with dsDNA in the absence of free

DNA ends that increased in magnitude with increasing Ku concentrations (Figure S5). This observation is consistent with computational and structural studies that have predicted a putative DNA-binding capacity of the SAP domain of Ku70.[41,42] We hypothesize that this background might be the result of non-specific transient interactions between the Ku70 SAP domain and the central dsDNA sequence of the construct.

Next, we performed the same assay adding 10 nM X4-LIG4, in excess with respect to the limiting concentration of Ku. Single-molecule FRET experiments have shown that Ku and X4-LIG4 are sufficient to achieve blunt-end synapsis in force-free experiments.[19,20] Moreover, some studies suggest that LIG4, in addition to its catalytic role in ligation, might also have a structural role supporting DNA end bridging.[16,43] However, our results showed an 89% probability of molecules being extended after incubation with Ku and X4-LIG4 (Figure 1D). The remaining probability was associated to a wide range of non-specific reductions ($\Delta z$) between $-0.3$ and $-0.1 \pm 0.02$ μm (Figure 1D). These non-specific reductions were also observed when the concentration of Ku was increased to 5 nM on an unbranched DNA (Figure S5). Under our assay conditions, Ku and X4-LIG4 were not sufficient for stable DNA end bridging, although X4-LIG4 amplified all DNA interactions by Ku, some of which might be synaptic. These results might contrast with single-molecule FRET experiments performed in the absence of force[20] and bulk ligation assays.[30] However, we interpret the lack of the synaptic peak as the consequence of the inherent pulling force of our assay (2 pN), which might be disrupting a transient bridging complex formed at low force by Ku and X4-LIG4. In support of this hypothesis, previous work using a similar MT setup did not find synapsis induced only by Ku and X4-LIG4.[40]

In contrast to X4-LIG4, the addition of 10 nM APLF to the 1 nM Ku assay showed multiple events consistent with specific DNA synapsis (Figure 1B). A clear reduction of extension was observed in some of the pulling cycles in multiple individual time courses obtained in the presence of Ku and APLF (Figures 1B, S6, and S7). This intermediate position, centered at $-0.2$ μm, corresponds to the configuration where the DNA ends are bridged and supported by the protein complex. Interestingly, the formation of the synaptic complex on the DNA ends could be also detected in the relaxation step, as the occurrence slightly shifted the molecule's fluctuations to lower values (Figures 1B [R] and S1B [arrow]). It was also noticeable that the synaptic complex could sometimes resist several consecutive pulling cycles until the bridge ruptured (Figures 1E and S7). In this experiment, about 62% of the molecules suffered some shortening event in at least one of the cycles (Figure S6). The relative reduction distribution showed a clear peak at $\Delta z = -0.19$ μm, from now on referred to as a synaptic peak, showing a 17% ± 2% of probability of the DNA ends being bridged (Figure 1E). Altogether our results demonstrate that APLF supports the bridging of DNA ends previously recognized by Ku. This was further supported by atomic force microscopy experiments showing that the addition of APLF to a mix of Ku with dsDNA is sufficient to induce the association between several fragments of DNA (Figures S3E–S3G).

Next, we studied the individual contribution of XLF to the bridging of DNA ends by performing the force cycles assay in the presence of 1 nM Ku and 5 nM XLF. The relative extension distribution showed no synaptic peak, but it did show a wide range of DNA extension reductions (Figure 1F). Around 77% of the molecules suffered some shortening event in at least one of the cycles (Figure S6). These non-specific shortenings likely arise from the interaction of XLF with Ku through the reported X-KBM present in XLF.[18]

To quantify the strength of the synapsis, we defined a dwell time, referred to as τ, as the time it takes for a synapsed molecule subjected to a pulling force to recover its original extension. τ distributions and averaged τ values were calculated and represented in a violin plot for Ku, Ku-X4-LIG4, Ku-APLF, and Ku-XLF combinations (Figure 1G, densities and circles). For Ku and Ku-X4-LIG4 the averaged τ values were 0.0 and 0.8 s, respectively, and for Ku-APLF and Ku-XLF, this shifted to $\tau = 2.2$ s (Figure 1G). The increase in the dwell time was similar for Ku-APLF and Ku-XLF; however, for APLF the interactions were specific to a synaptic state, while for XLF the interactions could resist the pulling force but were non-specific. Moreover, an additional experiment with longer pulling cycles showed that Ku-APLF sometimes secured the DNA end bridging for the 3-min duration of the steps (Figure S8).

We conclude that APLF is able to form and support a bridge between the ends of a DSB in the presence of Ku in a synaptic complex without the help of additional NHEJ factors. These results are unexpected as APLF has only one known Ku-binding motif (KBM) and no dsDNA binding capabilities.[30] Our results show that APLF contributes to the stability of synaptic events in coordination with Ku.

## The APLF C-terminal acidic domain is critical for DNA end bridging

To gain further insight into the bridging mechanism by APLF we performed MT experiments with APLF and Ku mutants. We produced a mutant Ku complex containing a deletion of the Ku80 C-terminal domain, which participates in DNA-PKcs recruitment but is dispensable for DNA end binding,[5] and a point mutation L68R in the Ku80 von Willebrand antigen (vWA) domain. This heterodimer (Ku70/Ku80$\Delta C^{L68R}$, referred to as $Ku^{L68R}$) has been shown to preserve the formation of the ring and to maintain its binding capability to dsDNA,[5,30] but loses the ability to interact with APLF through its KBM.[18,30] Consequently, EMSAs showed that this mutant binds to dsDNA but fails to recruit APLF (Figure S3B). Importantly, MT experiments using $Ku^{L68R}$ mutant and wild-type APLF did not result in synapses (Figure 2A). This demonstrates that the binding to the KBM is crucial for the bridging of DNA ends as APLF's inability to bind Ku abolishes synapses.

We also produced three APLF mutants that targeted its other defined regions. Two of them contained point mutations described previously to impair the interaction of the respective domain with its binding partner, one in the FHA domain ($APLF^{R27A}$) and the other in both PBZ domains ($APLF^{C387A-C427A}$, referred to as $APLF^{ZFD}$). For both mutants, we observed bridging of DNA ends in our MT assay in the presence of wild-type Ku (Figures 2B and 2C). This indicates that neither the FHA domain, which has been reported to interact with XRCC4,[26,28,29] nor the PBZs, which interact with PAR,[31,32]

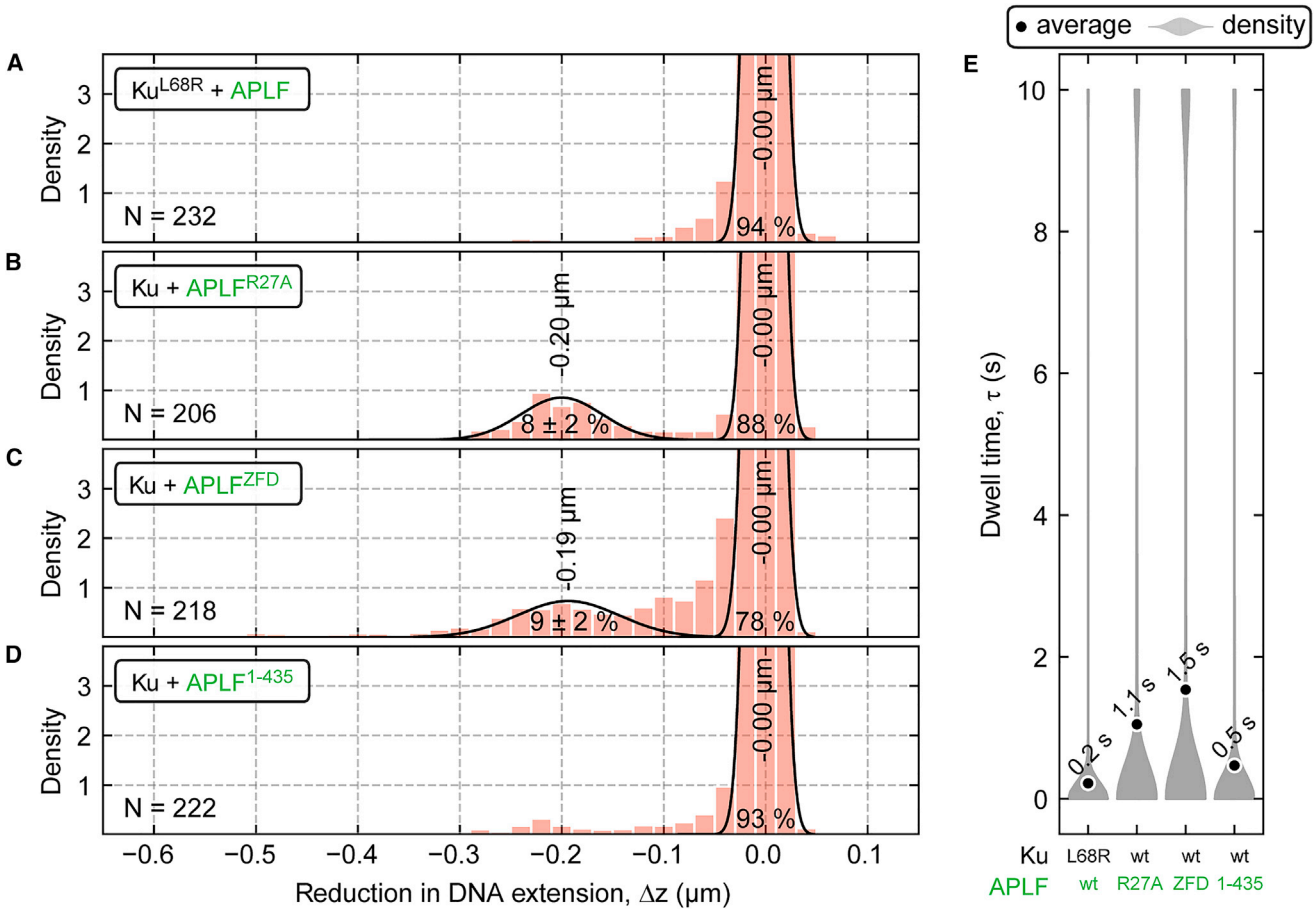


**Figure 2. The APLF C-terminal acidic domain is critical for DNA-end bridging**

(A–D) Relative reduction distributions for branched DNA molecules in the presence of Ku70/Ku80ΔC$^{L68R}$ mutant (Ku$^{L68R}$) and wild-type APLF (N = 232), wild-type Ku and APLF$^{R27A}$ mutant (N = 206), wild-type Ku and APLF$^{C387A–C427A}$ (APLF$^{ZFD}$) mutant (N = 218), and wild-type Ku and APLF$^{1-435}$ mutant (N = 222), respectively.

(E) Violin plot of the dwell time (τ) distribution for conditions in (A–D).

are involved in the bridging of Ku-bound DNA ends. A third mutant with a deletion of the C-terminal acidic domain was also studied (APLF$^{1-435}$). This region has been reported to be involved in the binding to histones.[33] Importantly, our data using APLF$^{1-435}$ showed that the lack of the acidic domain abolished the formation of stable synaptic events (Figure 2D). This observation contrasts with the results obtained for wild-type APLF (Figure 1E). The consequences of truncating the acidic domain are not related to defects in the recruitment of APLF to Ku since APLF$^{1-435}$ and Ku form a complex (Figure S3B), and instead suggests that the C-terminal acidic domain of APLF is also involved in the bridging of DNA-ends.

Together, we propose that APLF molecules bridge two Ku-bound DNA ends by binding to one Ku-DNA complex through the KBM, while probing for the other Ku-bound DNA end via its C-terminal acidic domain.

## APLF bridges DNA ends in the presence of X4-LIG4 and XLF

Once the individual contributions were established, we investigated the combined contributions of the different factors. Ku, X4-LIG4, and XLF are considered core factors of the NHEJ synaptic complex, and studies have shown that they are sufficient to bridge DNA ends.[19–21,30] To investigate the combined contributions of all these factors in our system, we reconstituted the synaptic complex with 1 nM Ku, 10 nM X4-LIG4, 5 nM XLF, and 10 nM APLF. From the relative reduction distribution, we could fit a synaptic peak with a 13% ± 1% of probability; however, the peak was hidden among non-specific reductions (Figure 3A, dashed line). Around 59% of the molecules suffered some shortening event in at least one of the cycles (Figure S6). The average τ was 1.9 s (Figure 3E). Then, we removed APLF from the protein complex and the synaptic peak disappeared (Figure 3B). This confirmed that the synaptic peak required the contribution of APLF. In addition, we observed that the high background of non-specific interactions disappeared when XLF was removed from the mix (Figure 3C). X4-L4 and XLF have been proposed to form fibers around DNA ends,[19] and it is tempting to speculate that the observed non-specific background arises from the parallel sliding between fibers. The probability for synapsis in the presence of Ku-X4-LIG4-APLF was slightly lower than for Ku and APLF (Figure 1E). This slight reduction was also observed

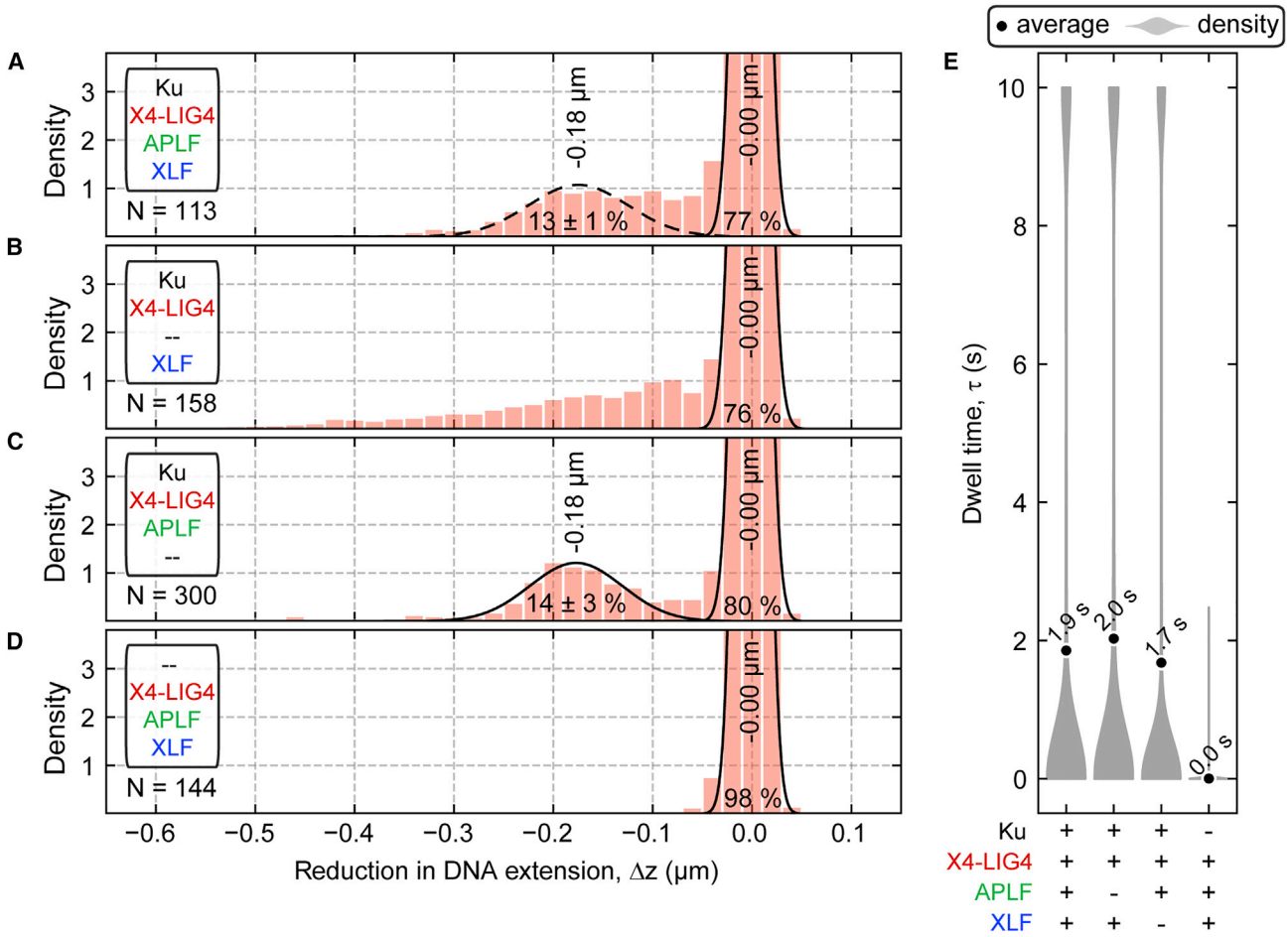


**Figure 3. APLF bridges DNA ends in the presence of X4-LIG4 and XLF**

(A–D) Relative reduction distributions for branched DNA molecules in the presence of the synaptic complex formed by Ku, X4-LIG4, APLF, and XLF (N = 113), without APLF (N = 158), without XLF (N = 300), and without Ku (N = 144), respectively.

(E) Violin plot of the dwell time (τ) distribution for conditions in (A–D).

in other conditions that include X4-LIG4, and might be due to steric hindrance effects. As expected, Ku was essential for all specific and non-specific interactions (Figure 3D; see Figure S7 for other representative time courses).

Taken together our results indicate that APLF promotes stable synapsis between DNA ends. In support of this, the addition of APLF to a ligation reaction, including Ku and X4-LIG4, greatly increased its efficiency (Figure S3C), as has been described previously.[30] Moreover, while not contributing to a specific interaction between the DNA ends, XLF did increase the dwell times of non-specific interactions, which could in turn further stabilize the bridging by other factors, which is in agreement with published data.[11,20] Finally, our results show that DNA end synapsis can occur in a DNA-PKcs-independent manner, consistent with previous works.[19–22]

## APLF bridging is disabled by the LR synaptic complex, including DNA-PKcs

To investigate the role that APLF could have in the LR synaptic complex, we reproduced key MT experiments, including DNA-PKcs in the reaction (Figure 4). The work by Chen et al.[11] determined the structure of a LR synaptic complex that brings two DNA ends into proximity and an SR synaptic complex in which the DNA ends are aligned and ready for ligation. The LR complex includes Ku, DNA-PKcs, X4-LIG4, and XLF, and DNA ends are held approximately 11.5 nm apart. The transition from the LR to the SR configuration is induced by the autophosphorylation of DNA-PKcs, which leads to its dissociation from the synaptic complex. Thus, the SR complex does not contain DNA-PKcs and brings the two DNA ends much closer in a position ready for ligation. In the literature, studies of APLF *in vitro* have mostly focused in reactions lacking DNA-PKcs.[44]

To focus on the role of APLF alongside DNA-PKcs in the LR complex, we performed new MT experiments in the absence of ATP to prevent autophosphorylation of DNA-PKcs. Ku and DNA-PKcs alone were not able to generate stable synapsis in our MT assay (Figure 4A). This is consistent with the work of Wang et al.,[40] where a similar assay was employed and could only observe very short-lived (100 ms) synaptic events. The addition of the two other components of the LR synaptic complex, XLF

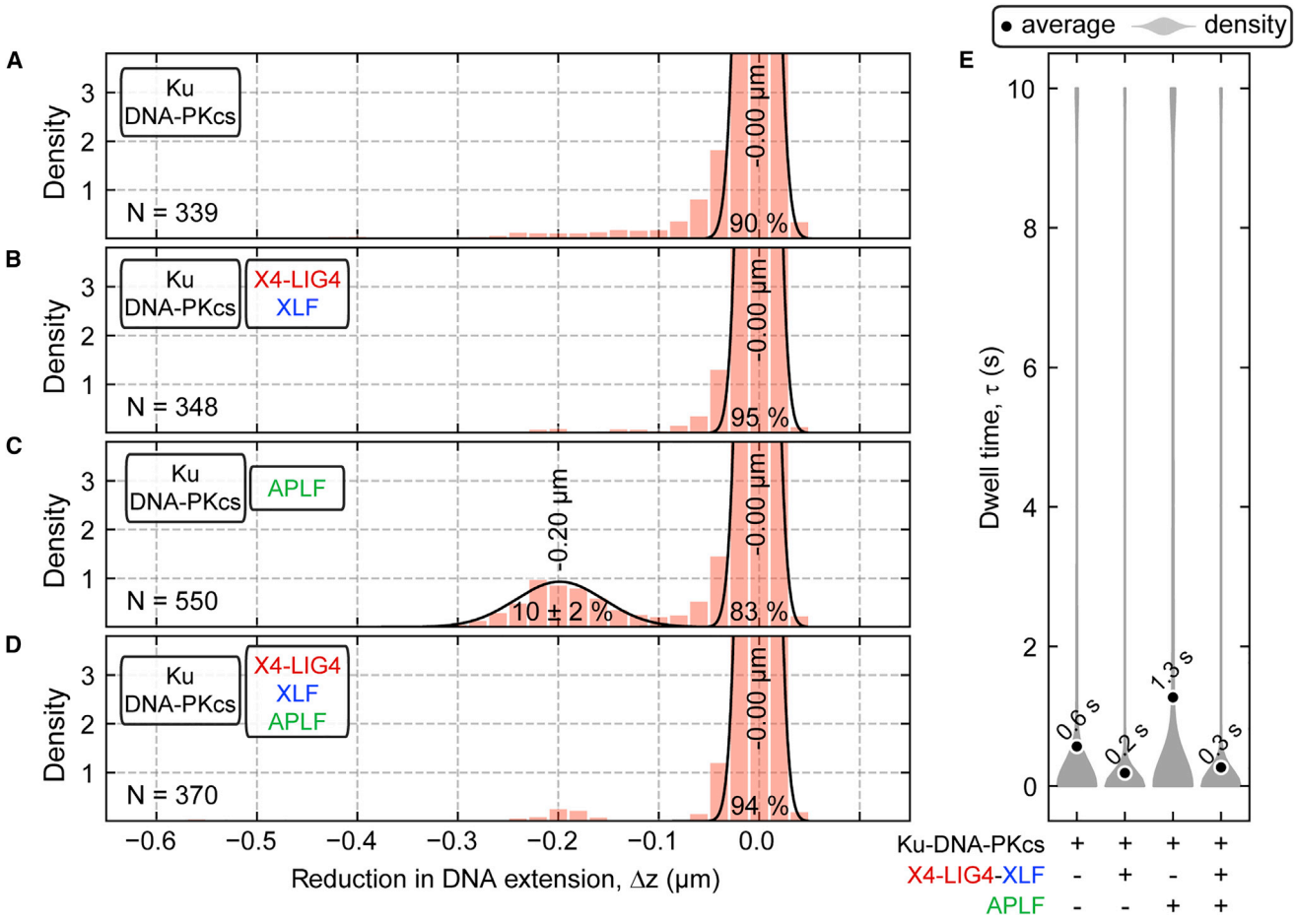


**Figure 4. APLF bridging is disabled by the long-range synaptic complex, including DNA-PKcs**

(A–D) Relative reduction distributions for branched DNA molecules in the presence of Ku and DNA-PKcs (N = 339), Ku, DNA-PKcs, X4-LIG4, and XLF (N = 348), Ku, DNA-PKcs, and APLF (N = 550), and Ku, DNA-PKcs, X4-LIG4, XLF, and APLF (N = 370), respectively.

(E) Violin plot of the dwell time (τ) distribution for conditions in (A–D).

and X4-LIG4, did not increase the stability of the bridging by the synaptic complex (Figure 4B), also in agreement with Wang et al. Moreover, the direct comparison with the experiment where DNA-PKcs was absent (Figure 3B) suggests that DNA-ends are blocked by DNA-PKcs, which prevents the non-specific transient interactions between DNA ends and other parts of the DNA construct.

Notably, addition of APLF to the minimum reaction containing Ku and DNA-PKcs resulted in seconds-long synaptic events (Figure 4C) but with a lower probability compared with the experiment performed with only Ku and APLF (Figure 1E). This result is consistent with APLF-mediated bridging but also suggests a likely competition between DNA-PKcs and APLF for binding to Ku. It is also worth mentioning that the distance between Ku-bound DNA ends in LR synapsis of 11.5 nm might be too large to be linked by single APLF molecules. Interestingly, inclusion of X4-LIG4 and XLF to allow formation of the full LR complex precluded the formation of stable synapsis in the presence of APLF (Figure 4D), in contrast to what was observed without DNA-PKcs (Figure 3A). This could be explained by further blockage of Ku for APLF binding, and/or, as indicated above, by the excessive distance between DNA ends expected in the LR synaptic complex.

Together these data suggest that APLF might not play a role at the synapsis established by the LR complex, where the two DNA ends are weakly linked by Ku, DNA-PKcs, X4-LIG4, and XLF. Upon dissociation of DNA-PKcs and the transition to the SR stage, APLF plays the role of stabilizing the bridging between the DNA ends, facilitating ligation.

## lncRNA NIHCOLE stabilizes DNA ends bridging by Ku and APLF

In our previous work, we described how NIHCOLE, a lncRNA overexpressed in hepatocellular carcinoma, positively contributes to the NHEJ pathway by enhancing DSB ligation efficiency.[38] To gain more insight into how NIHCOLE promotes ligation, we studied whether NIHCOLE contributes to the formation or stability of the synaptic complex.

As DNA end bridging was predominantly mediated by APLF, we performed the assay with 1 nM Ku, 10 nM APLF, and 10 nM lncRNA NIHCOLE. The presence of NIHCOLE significantly

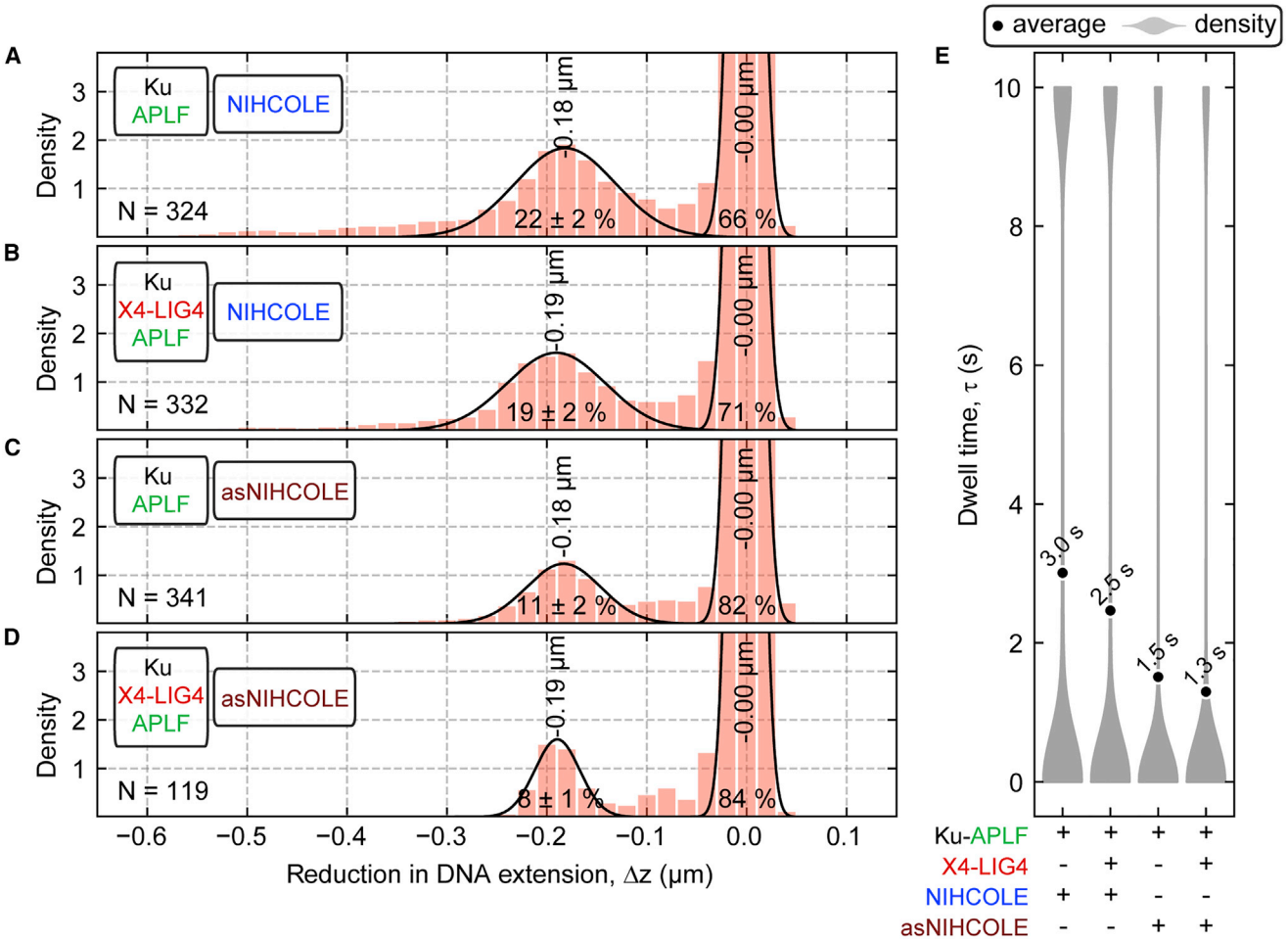


**Figure 5. lncRNA NIHCOLE stabilizes DNA end bridging by Ku and APLF**

(A and B) Relative reduction distributions for branched DNA molecules in the presence of lncRNA NIHCOLE and the protein complex formed by Ku-APLF (N = 324), and Ku-APLF with X4-LIG4 (N = 332), respectively.

(C and D) Relative reduction distributions for branched DNA molecules in the presence of antisense NIHCOLE (asNIHCOLE) and the protein complex formed by Ku-APLF (N = 341), and Ku-APLF with X4-LIG4 (N = 119), respectively.

(E) Violin plot of the dwell time (τ) distribution for conditions in (A–D).

increased the DNA end bridging probability to 22% ± 2%, while also increasing the number of non-specific interactions (Figures 5A and S9). About 71% of the molecules suffered some shortening event in at least one of the cycles (Figure S6). The presence of NIHCOLE also increased the strength of the interactions. The number of bridging events lasting at least 10 s (a time limitation imposed in our assay) increased and the averaged τ shifted from τ = 2.2 to 3.0 s (Figure 5E). In the absence of APLF or using NIHCOLE only, no specific DNA bridging was observed (Figures S4D and S4E), negating the possibility of bridging mediated by the RNA alone. We next explored the potential role of X4-LIG4 in the presence of NIHCOLE. The results obtained were similar to only adding Ku and APLF (Figures 5B and S6), confirming the residual role of X4-LIG4 in our system. Importantly, a control experiment, including 10 nM antisense NIHCOLE (asNIHCOLE), showed a slight reduction of bridging probability from 17% to 11% ± 2% (Figure 5C), and an averaged τ value reduction from 2.2 to 1.5 s (Figures 5E and S6). This reduction might be the result of the competition between DNA and RNA for Ku, as Ku also binds RNA hairpins.[45,46] Consistent with our previous finding, including 10 nM X4-LIG4 did not change the negative effect asNIHCOLE had on the DNA bridging (Figure 5D), and the averaged τ remained almost the same (Figures 5E and S6). In summary, addition of NIHCOLE increased the probability of bridging as well as the resistance of the synapsis and this interaction was specific because a control RNA did not promote nor strengthen the synapsis (Figure 5E). The observed additional stability mediated by NIHCOLE could explain the improved ligation efficiency that we reported previously in bulk assays.[38]

## A small structural domain of lncRNA NIHCOLE is sufficient to strengthen the NHEJ synaptic complex

It has been described that Ku can bind to RNA hairpins,[45,46] and NIHCOLE has been predicted to fold into stable stem-loop

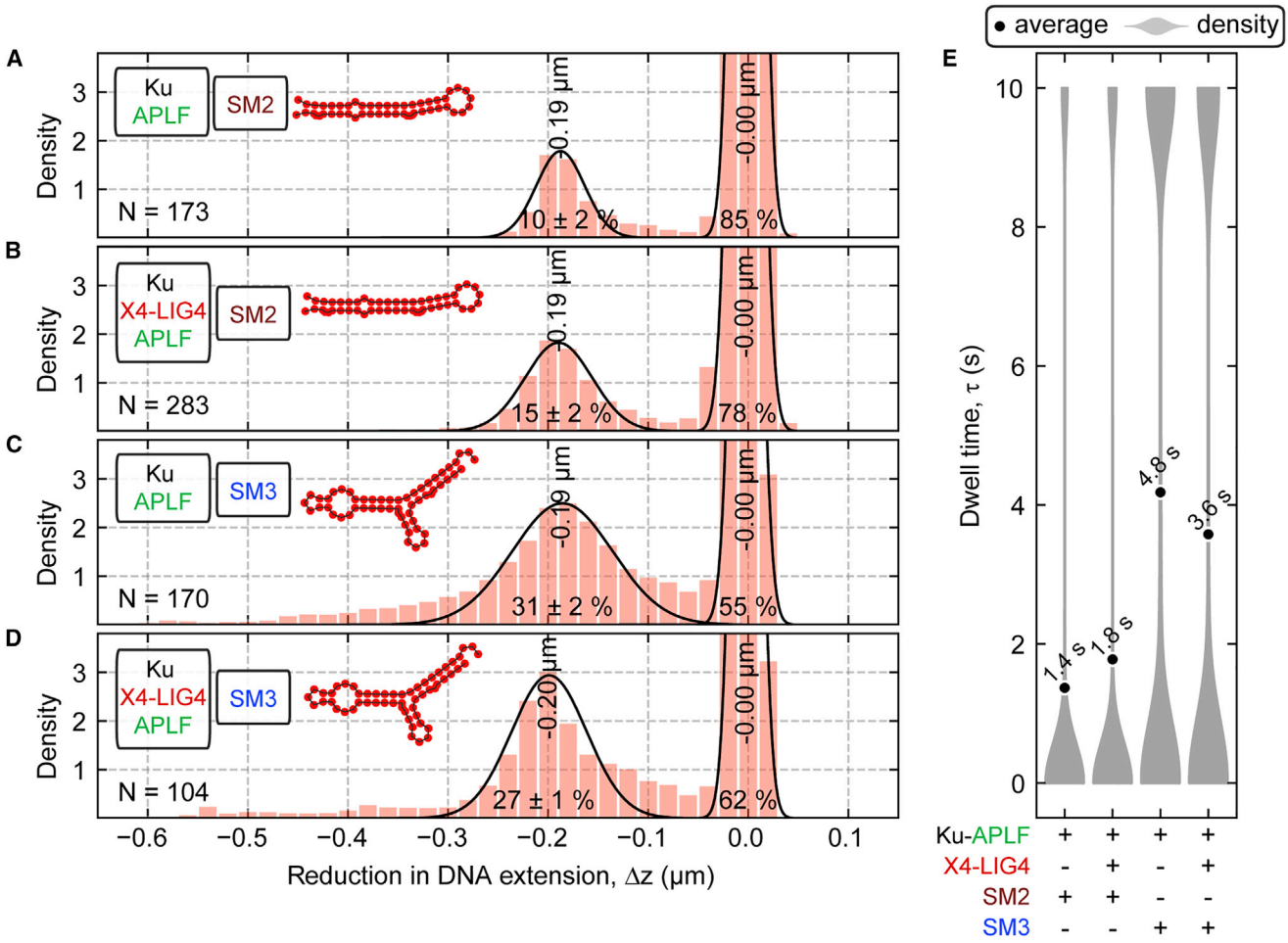


**Figure 6. SM3 structural domain of lncRNA NIHCOLE is sufficient to strengthen the NHEJ synaptic complex**

(A and B) Relative reduction distributions for branched DNA molecules in the presence of the fragment SM2 and the protein complex formed by Ku-APLF (N = 173), and Ku-APLF with X4-LIG4 (N = 283), respectively.

(C and D) Relative reduction distributions for branched DNA molecules in the presence of the fragment SM3 and the protein complex formed by Ku-APLF (N = 170), and Ku-APLF with X4-LIG4 (N = 104), respectively.

(E) Violin plot of the dwell time (τ) distribution for conditions in (A–D).

structures, including structural motifs 2 and 3 (SM2 and SM3).[38] SM2 is 50 nucleotides long and has a predicted rod-like structure while SM3 is a 56-nucleotide-long molecule with a putative fork-like shape. We have shown previously that, although SM2 and SM3 bind to Ku in EMSAs with good affinity, only SM3 can form a stable trimeric complex with APLF that can be recognized by X4-LIG4.[38] We hypothesized that Ku binding to NIHCOLE SMs could promote synapsis in NHEJ.

To test this hypothesis, we first performed the bridging assay by adding 1 nM Ku, 10 nM APLF, and 10 nM SM2. The probability of having the branches bridged dropped from 17% to 10% ± 2% in the presence of SM2 (compare Figure 1E with Figure 6A) and the averaged τ dropped from 2.2 to 1.4 s (Figures 6E and S6). A similar result was obtained when adding 10 nM X4-LIG4 (Figures 6B and 6E). This decrease of synapsis probability might reflect a competition between the DNA ends and SM2 for Ku. In contrast to SM2, 10 nM SM3 significantly enhanced DNA end bridging from 17% to 31% ± 2% (Figure 6C). Notably, the number of synaptic events lasting for 10 s escalated and the average τ doubled from 2.2 to 4.8 s (Figure 6E). In these experiments, 81% of the molecules displayed some shortening event in at least one of the cycles (Figure S6). The enhancing effect observed with SM3 was reproduced in an additional experiment including 10 nM X4-LIG4 (Figures 6D and 6E). See supplemental information for examples of individual traces (Figure S9). In summary, our results demonstrate that a small structural motif within lncRNA NIHCOLE is sufficient to promote DNA end synapsis in the presence of Ku and enhance the effects of APLF.

## DISCUSSION

### APLF effectively bridges highly mobile DNA ends

We report here evidence that APLF mediates the synapsis of blunt DNA ends after their recognition by Ku heterodimers and

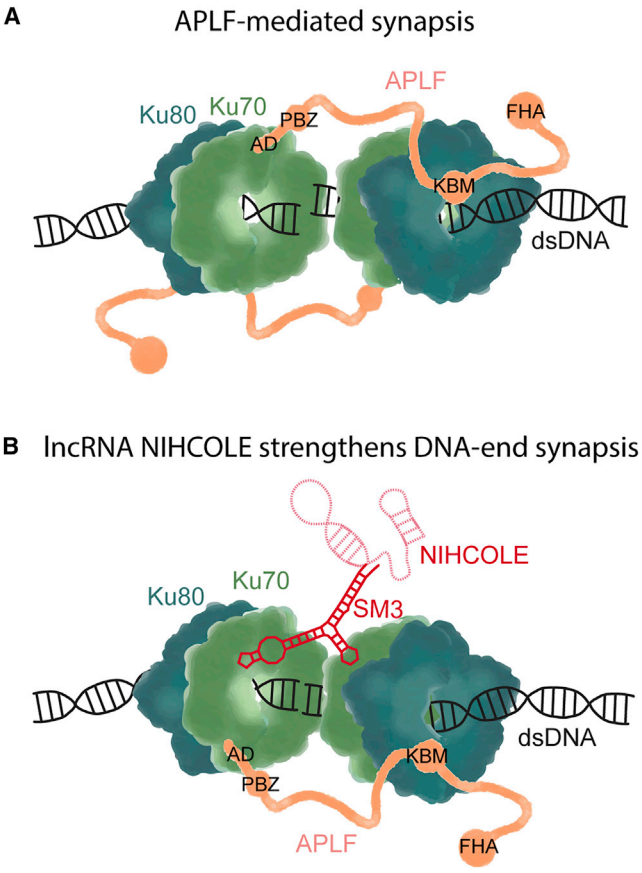


**Figure 7. Role of APLF and lncRNA NIHCOLE in NHEJ synaptic complex**

(A) APLF-mediated synapsis. One APLF molecule interacts with the Ku80 subunit of one Ku-DNA complex via its KBM, while its C-terminal acidic domain ($APLF^{AD}$, indicated as AD) interacts with the other Ku-DNA complex. (B) lncRNA NIHCOLE, through its SM3 domain, strengthens the APLF-mediated synapsis (see discussion).

secures the bridging even when subjected to a pulling force. Our assay allowed us to monitor individual molecules and assess the relative lifetime of the bridging events at a given opposing force. The synaptic conformation by Ku-APLF could resist forces in the piconewton range for several consecutive force cycles before rupture, resisting up to 3 min under stress (Figure S8). Wang et al., in previous work, found a minimal combination of Ku, DNA-PKcs, and PAXX to be necessary for transient bridging of dephosphorylated blunt DNA ends. The averaged dwell time of the bridging events was 2.2 s for pulling cycles at 1.4 pN lasting 225 s.[40] Here, we report that APLF and Ku stabilize DNA bridging to a greater extent than Ku, DNA-PKcs, and PAXX.[40] Our experiments also show that Ku and DNA-PKcs cannot form stable synapsis, but that these are recovered in the presence of APLF, similarly to the reported effect of PAXX.[40] Interestingly, the synapsis is lost when the other components X4-LIG4 and XLF are included, suggesting that APLF does not play a role in the formation of the LR complex, which includes DNA-PKcs.

Ku, X4-LIG4, and XLF have been shown to be essential for NHEJ, but the role of DNA-PKcs in synapsis formation is controversial. DNA-PKcs is required for the establishment of the LR complex,[11,16] and DNA-PKcs kinase activity is needed for the transition to the SR state complex in *Xenopus* extracts.[11] However, a recent work demonstrates that DNA-PKcs and the formation of the LR complex is not absolutely required for end joining of blunt chromosomal DSBs.[22] Instead, DNA-PKcs only becomes important when using XLF mutants with disrupted binding interfaces. Functional redundancies between DNA-PKcs and XLF have also been described during V(D)J recombination, where DNA end joining is abolished only when both proteins are mutated.[47] Based on these findings, it has been proposed that the need for DNA-PKcs during NHEJ would be dependent on the specific circumstance.[22] Our work correlates well with these cellular observations by showing that an SR complex can be assembled on DNA ends using purified proteins without the need for DNA-PKcs, and by demonstrating that synapses can occur in a DNA-PKcs independent manner. Our assay establishes a minimal combination of NHEJ proteins able to support blunt DNA end synapsis for several minutes under applied forces.

To date, APLF has been considered an accessory factor for NHEJ.[28,48] However, the stable and strong ends bridging observed in this work mediated by only Ku and APLF raises some questions about whether APLF's function is more relevant than suggested previously. Biochemical assays performed in this work (Figure S3C) and by Grundy et al. demonstrated that APLF amplifies the ligation efficiency by Ku and X4-LIG4 and that this seems to occur because APLF stabilizes the interaction between Ku and X4-LIG4 required for ligation.[30] Moreover, the depletion of APLF in human and avian DT40 cells leads to defects in the ligation of plasmids and to a reduction of repair rate after DNA damage.[26,28–30,48] Still, DNA ligation is possible with only Ku and X4-LIG4, as demonstrated in bulk[20,30,49] and force-free single-molecule FRET.[19–21] In cells, exposed DNA ends from physiological DSBs usually remain in close proximity right after damage and this might facilitate the ligation of DSBs by Ku and X4-LIG4 alone. However, limited mobility due to the chromosomal packaging is only applicable to certain DNA breaks.[50] The nucleus is a dynamic environment and DNA transport is particularly relevant after DSBs. Under these circumstances, the role of APLF may be essential to keep the two broken DNA ends together under the mechanical forces that lead to DNA motion. Such physiological conditions could be mimicked, in part, by our MT assay, where the bridging is subjected to an opposing force, and this limits the bridging to only the most stable combination of proteins. Indeed, the complex formed by Ku and X4-LIG4 was not able to form synapses resistant to a pulling force of 2 pN. However, we did observe the formation of multiple transient non-specific DNA-DNA interactions, which were further enhanced by the binding of XLF. This could be explained by the formation of protein fibers on the DNA ends that allow the ends to slide alongside each other.[19]

In this context of high DNA end mobility and resistance to force, we propose a scouting role for APLF, probing for interactions within a short range, and a scaffolding role, securing the synaptic complex and reducing the DNA end mobility. In our model, APLF would form a flexible synaptic complex with two Ku heterodimers, each anchored to a DNA end (Figure 7A). APLF flexibility would act like a safety belt that assists the core

NHEJ complex to avoid separation of DNA ends, reinforcing and reinsuring the correct ligation of the DSB ends. The supporting mechanism for APLF bridging is nevertheless unclear. APLF has only one reported Ku-binding motif (A-KBM),[18,29,44] which is not enough for the bridging of both ends of a DSB. We disturbed this known interaction between APLF and Ku by mutating the vWA region of Ku80, which is responsible for binding to APLF (Ku70/Ku80ΔC$^{L68R}$). As expected, experiments with Ku70/Ku80ΔC$^{L68R}$ did not show bridging, therefore confirming this region in Ku to be critical for bridging by APLF. Subsequently, to explore the role in bridging of the other regions of APLF, we generated three APLF mutants. Neither mutations in the FHA nor PBZ domains of APLF affected bridging. However, deletion of the C-terminal acidic domain severely affected the formation of synapses. APLF's intrinsically disordered regions (IDRs) might be behind its cryptic function.[25] The C-terminal acidic region of APLF is itself an IDR, and IDR regions, due to their flexibility, have been suggested to facilitate interactions with multiple partners through intra- and intermolecular mechanisms.[51] Reconstructed models of several complexes between Ku and APLF based on the constraints of small-angle X-ray scattering (SAXS) data revealed that the APLF acidic domain is flexible and exposed when in complex with Ku and X4-LIG4,[25] and therefore it is conceivable that, if APLF interacts with Ku, its C-terminal end can reach the other end of the break. Interestingly, a recent structure reveals how residues D482-P487 of APLF interact with histones H2A-H2B of the nucleosome, whereas residues P459-D471 interact with H3-H4,[33,34] demonstrating that the acidic region of APLF can be involved in distinct protein-protein interactions. Thus, we propose a model where the KBM of APLF is recruited to one Ku, allowing its flexible acidic domain to interact with another Ku at the opposite end of the break (Figure 7A).

### Synaptic reinforcement by lncRNA NIHCOLE

Cumulative evidence shows that some lncRNAs are implicated in DNA repair pathways.[35–38] In previous work, we identified the lncRNA NIHCOLE as an enhancing factor to the ligation efficiency of DSBs by NHEJ.[38] The mechanisms for this are unclear, but since this lncRNA could bind multiple Ku molecules, we proposed that NIHCOLE could serve to provide a pool of Ku and other NHEJ factors near the site of damage. We report here that the lncRNA NIHCOLE enhances DNA end synapsis and fortifies the bridging by the NHEJ synaptic complex, and that the SM3 structural motif of NIHCOLE is sufficient to explain these effects. Similar results have been reported by Thapar et al. using a similar technique as in this work, where LINP1 lncRNA was shown to increase the lifetime of the synaptic complex by Ku and DNA-PKcs from milliseconds to 4.8 s at a pulling force of 1.4 pN.[36] Importantly, our work differs in that we observe interaction in a DNA-PKcs-independent manner. This proves that the DSB repair enhancement by the lncRNAs comes from their interaction with Ku alone, rather than through DNA-PKcs.

The precise mechanism through which NIHCOLE, and in particular the SM3 domain, strengthens the DNA end bridging is unclear. Previous experiments showed that NIHCOLE can interact with several copies of Ku, that SM3 could promote the interaction between two Ku molecules, and that the complex between Ku and SM3 was compatible with the binding to APLF. In addition, SAXS experiments using Ku and a fragment of LINP1 indicate that the preformed ring that binds DNA in the Ku heterodimer can also bind RNA.[36] These findings are consistent with the idea that the ring structure of Ku binds dsRNA structures independent of their sequence.[45,46] Indeed, the ring region of yeast Ku binds telomeric RNA.[52] However, the binding of Ku to RNA using the same ring structure as for the recognition of DSBs would make the binding of Ku to the DNA and NIHCOLE mutually exclusive. All this evidence suggested that NIHCOLE could work by providing an enriched pool of Ku and potentially other factors, such as APLF, that somehow would facilitate NHEJ, but each Ku molecule would only bind directly to either RNA or a DNA end at the break.[38] The proposal of "condensates" formed by Ku and lncRNAs has also been suggested for LINP1.[36] However, our results here clearly demonstrate that the small structural domain SM3 is sufficient to recapitulate the activity of NIHCOLE, enhancing synapsis. This finding is difficult to reconcile with the model of the condensate. On the one hand, the small size of these RNA fragments disfavors direct large-scale scaffolding or multimerization of Ku molecules. On the other hand, SM3 has a strong effect in enhancing DNA end bridging and the number of synaptic events lasting for 10 s or more, and this is only manifested when Ku and APLF are present. All this is hardly compatible with a model where the RNA just serves as a "stock" of Ku molecules near the DNA break. Thereby our results strongly support a model where Ku can coexist in a complex with APLF and SM3 (or NIHCOLE) while bound to the dsDNA end.

The possibility that Ku can bind DNA and RNA simultaneously requires distinct binding sites for each. In support of this idea, Anisenko et al. biochemically demonstrated that Ku70 presents a high affinity for RNA hairpins.[45] This could be the case of SM3 given its fork-like structure in contrast with the more rod-like shape of SM2. Anisenko et al. also showed that the binding mechanism for the human Ku70 subunit is different from the one established for the Ku heterodimer. Ku70 binds RNA and DNA through two different binding sites: the dsDNA recognized by the C-terminal part of Ku70, including the SAP domain,[42,45] whereas the RNA hairpin binds a specific site in the Ku70 inner ring.[45] In addition, they also demonstrated that, among several RNA structures, only RNA hairpins with a fork-like structure, similar to SM3, were able to bind to Ku70.[45] This fork-like secondary structure has also been described for HIV TAR RNA; another RNA hairpin known to bind to the Ku heterodimer.[53] Although these findings do not apply directly to Ku heterodimers, they suggest that, when Ku binds dsDNA, other regions could potentially bind RNA.

In this scenario of a Ku-APLF-SM3 complex on DNA, SM3 could be facilitating the scaffolding of the synaptic site by interacting with each Ku molecule at each end of the DSB (Figure 7B). SM3 contains two hairpins that might facilitate the formation of a dimer of Ku heterodimers. In fact, EMSA experiments using Ku and SM3 show two supershifted complexes (Figure S3D),[38] suggesting that SM3 fragments can facilitate the interaction between two Ku molecules. Alternatively, considering the small size of the RNA domains, SM3 may be promoting conformational changes in the Ku heterodimer that could lead to a stronger complex and enhanced resistance of the synaptic complex to pulling forces (Figure 7B). These conformational changes could be

promoting the interaction between the NHEJ factors at both ends of the break or enhancing the DNA-binding affinity in the Ku heterodimer. In both cases, the Ku heterodimer needs to be part of a complex where binding to DNA and RNA coexists, and this is something that has not been reported to date.

Our findings reinforce the notion that the NHEJ reaction is remarkably versatile and that multiple processing enzymes and regulatory factors can be recruited by the core NHEJ machinery. DNA-PKcs is not a mandatory element to achieve synapsis in agreement with recent experiments performed in cells.[22] The single-molecule experiments described in this work reveal that the interaction of APLF and lncRNA NIHCOLE with some of the core components serves to reinforce DNA-end synapsis during NHEJ.

### Limitations of the study

Our study has some limitations. We have used blunt DNA ends but DNA breaks arising in a biological context frequently show other chemistries and likely ends must be processed prior ligation. How the nature of these DNA ends affects the role of APLF and NIHCOLE lncRNA in synapsis will require additional studies. Moreover, experiments with multiple factors (protein and/or RNAs) are more difficult to interpret as reductions of DNA extension in MT and complementary approaches will be needed to understand how APLF and lncRNAs regulate the formation of the NHEJ synaptic complex. In addition, the results we show here represent only a few snapshots of the intricate regulation of NHEJ. For example, PAXX, a paralog of XRCC4 and XLF that interacts with Ku, has been described to contribute to the stabilization of DNA end synapses in similar single-molecule experiments,[40] but how the functions of PAXX overlap with those of APLF, what the interplay between all these different factors is, and if they can coexist in the same DNA break or rather they compete for binding, remains to be determined.

## STAR★METHODS

Detailed methods are provided in the online version of this paper and include the following:



## SUPPLEMENTAL INFORMATION

Supplemental information can be found online at https://doi.org/10.1016/j.celrep.2022.111917.

## ACKNOWLEDGMENTS

We acknowledge the help of Prof. Laurence H. Pearl (University of Sussex) in the production of all the NHEJ factors used in this work, with the exception of DNA-PKcs, kindly purified and donated to us by Prof. Susan P. Lees-Miller (University of Calgary). We also thank Ana Gonzalez Corpas at CNIO for her help with EMSA experiments.

This work was funded by grants PID2020-114429RB-I00 to O.L., PID2020-112998GB-I00 (open access) to F.M.-H., RTI2018-101759-B-I00 to P.F., and PID2021-1287910B-I00 to P.F., funded by Ministerio de Ciencia e Innovación (MICINN)/Agencia Estatal de Investigación (AEI/10.13039/501100011 033) _FEDER, EU, and co-funded by the European Regional Development Fund (ERDF); grants Y2018/BIO4747 and P2018/NMT4443 to both O.L. and F.M.-H., funded by the Autonomous Region of Madrid and co-funded by the European Social Fund (ESF) and the ERDF; grant EUREXCEL ref. 951214 to F. M.-H., funded by the CSIC; grant AECC IDEAS20169FORT to P.F., funded by the Scientific Foundation of the Spanish Association Against Cancer, and by the Instituto de Salud Carlos III (ISCIII), which supports CNIO, CIBEREhd, and TERAV ISCIII, funded by the European Union – NextGenerationEU, Plan de recuperación Transformación y Resiliencia.

J.P.U. is a recipient of the Azrieli Foundation International Postdoctoral Fellowship, the Excellence Fellowship Program for International Postdoctoral from Israel CHE/IASH, and an EMBO Postdoctoral Fellowship. L.P.M. is a recipient of a PFIS fellowship (FI20/00074) by the ISCIII and ESF "Investing in Your Future". M.M.-B. acknowledges support from MICINN as a recipient of an FPI fellowship (PRE2018-083464).

## AUTHOR CONTRIBUTIONS

S.d.B. performed all single-molecule experiments and analysis of data. C.A.-R. designed and fabricated DNA substrates for MT experiments. C.A.-R., R.A.-B., A.R.-C., J.P.-U., L.P.-M., and P.F. produced proteins, lncRNAs, and tested interaction and ligation efficiency between NHEJ factors in bulk. M.M.-B. performed atomic force microscopy imaging. O.L. and F.M.-H. designed the research. F.M.-H. and S.d.B. prepared the first version of the manuscript and figures. All authors revised and approved the manuscript.

## DECLARATION OF INTERESTS

The authors declare no competing interests.

## INCLUSION AND DIVERSITY

One or more of the authors of this paper self-identifies as a member of the LGBTQIA+ community. One or more of the authors of this paper self-identifies as an underrepresented ethnic minority in their field of research or within their geographical location.

Received: June 8, 2022
Revised: October 26, 2022
Accepted: December 13, 2022

## REFERENCES

1. Krenning, L., van den Berg, J., and Medema, R.H. (2019). Life or death after a break: what determines the choice? Mol. Cell *76*, 346–358. https://doi.org/10.1016/j.molcel.2019.08.023.

2. Lees-Miller, S.P., and Meek, K. (2003). Repair of DNA double strand breaks by non-homologous end joining. Biochimie *85*, 1161–1173. https://doi.org/10.1016/j.biochi.2003.10.011.

3. Stinson, B.M., and Loparo, J.J. (2021). Repair of DNA double-strand breaks by the nonhomologous end joining pathway. Annu. Rev. Biochem. *90*, 137–164. https://doi.org/10.1146/annurev-biochem-080320-110356.

4. Lieber, M.R. (2010). The mechanism of double-strand DNA break repair by the nonhomologous DNA end-joining pathway. Annu. Rev. Biochem. *79*, 181–211. https://doi.org/10.1146/annurev.biochem.052308.093131.

5. Walker, J.R., Corpina, R.A., and Goldberg, J. (2001). Structure of the Ku heterodimer bound to dna and its implications for double-strand break repair. Nature *412*, 607–614. https://doi.org/10.1038/35088000.

6. Sibanda, B.L., Critchlow, S.E., Begun, J., Pei, X.Y., Jackson, S.P., Blundell, T.L., and Pellegrini, L. (2001). Crystal structure of an Xrcc4–DNA ligase IV complex. Nat. Struct. Biol. *8*, 1015–1019. https://doi.org/10.1038/nsb725.

7. Wu, P.-Y., Frit, P., Meesala, S., Dauvillier, S., Modesti, M., Andres, S.N., Huang, Y., Sekiguchi, J., Calsou, P., Salles, B., and Junop, M.S. (2009). Structural and functional interaction between the human DNA repair proteins DNA ligase IV and XRCC4. Mol. Cell Biol. *29*, 3163–3172. https://doi.org/10.1128/MCB.01895-08.

8. Andres, S.N., Modesti, M., Tsai, C.J., Chu, G., and Junop, M.S. (2007). Crystal structure of human XLF: a twist in nonhomologous DNA end-joining. Mol. Cell *28*, 1093–1101. https://doi.org/10.1016/j.molcel.2007.10.024.

9. Andres, S.N., Vergnes, A., Ristic, D., Wyman, C., Modesti, M., and Junop, M. (2012). A human XRCC4-XLF complex bridges DNA. Nucleic Acids Res. *40*, 1868–1878. https://doi.org/10.1093/nar/gks022.

10. Li, Y., Chirgadze, D.Y., Bolanos-Garcia, V.M., Sibanda, B.L., Davies, O.R., Ahnesorg, P., Jackson, S.P., and Blundell, T.L. (2008). Crystal structure of human XLF/Cernunnos reveals unexpected differences from XRCC4 with implications for NHEJ. EMBO J. *27*, 290–300. https://doi.org/10.1038/sj.emboj.7601942.

11. Chen, S., Lee, L., Naila, T., Fishbain, S., Wang, A., Tomkinson, A.E., Lees-Miller, S.P., and He, Y. (2021). Structural basis of long-range to short-range synaptic transition in NHEJ. Nature *593*, 294–298. https://doi.org/10.1038/s41586-021-03458-7.

12. Chaplin, A.K., Hardwick, S.W., Stavridi, A.K., Buehl, C.J., Goff, N.J., Ropars, V., Liang, S., De Oliveira, T.M., Chirgadze, D.Y., Meek, K., et al. (2021). Cryo-EM of NHEJ supercomplexes provides insights into DNA repair. Mol. Cell *81*, 3400–3409.e3. https://doi.org/10.1016/j.molcel.2021.07.005.

13. Chaplin, A.K., Hardwick, S.W., Liang, S., Kefala Stavridi, A., Hnizda, A., Cooper, L.R., De Oliveira, T.M., Chirgadze, D.Y., and Blundell, T.L. (2021). Dimers of DNA-PK create a stage for DNA double-strand break repair. Nat. Struct. Mol. Biol. *28*, 13–19. https://doi.org/10.1038/s41594-020-00517-x.

14. Liu, L., Chen, X., Li, J., Wang, H., Buehl, C.J., Goff, N.J., Meek, K., Yang, W., and Gellert, M. (2022). Autophosphorylation transforms DNA-PK from protecting to processing DNA ends. Mol. Cell *82*, 177–189.e4. https://doi.org/10.1016/j.molcel.2021.11.025.

15. Watanabe, G., Lieber, M.R., and Williams, D.R. (2022). Structural analysis of the basal state of the Artemis:DNA-PKcs complex. Nucleic Acids Res. *50*, 7697–7720. https://doi.org/10.1093/nar/gkac564.

16. Graham, T.G.W., Walter, J.C., and Loparo, J.J. (2016). Two-stage synapsis of DNA ends during non-homologous end joining. Mol. Cell *61*, 850–858. https://doi.org/10.1016/j.molcel.2016.02.010.

17. Graham, T.G.W., Carney, S.M., Walter, J.C., and Loparo, J.J. (2018). A single XLF dimer bridges DNA ends during nonhomologous end joining. Nat. Struct. Mol. Biol. *25*, 877–884. https://doi.org/10.1038/s41594-018-0120-y.

18. Nemoz, C., Ropars, V., Frit, P., Gontier, A., Drevet, P., Yu, J., Guerois, R., Pitois, A., Comte, A., Delteil, C., et al. (2018). XLF and APLF bind Ku80 at two remote sites to ensure DNA repair by non-homologous end joining. Nat. Struct. Mol. Biol. *25*, 971–980. https://doi.org/10.1038/s41594-018-0133-6.

19. Reid, D.A., Keegan, S., Leo-Macias, A., Watanabe, G., Strande, N.T., Chang, H.H., Oksuz, B.A., Fenyo, D., Lieber, M.R., Ramsden, D.A., and Rothenberg, E. (2015). Organization and dynamics of the nonhomologous end-joining machinery during DNA double-strand break repair. Proc. Natl. Acad. Sci. USA *112*, E2575–E2584. https://doi.org/10.1073/pnas.1420115112.

20. Zhao, B., Watanabe, G., Morten, M.J., Reid, D.A., Rothenberg, E., and Lieber, M.R. (2019). The essential elements for the noncovalent association of two DNA ends during NHEJ synapsis. Nat. Commun. *10*, 3588. https://doi.org/10.1038/s41467-019-11507-z.

21. Conlin, M.P., Reid, D.A., Small, G.W., Chang, H.H., Watanabe, G., Lieber, M.R., Ramsden, D.A., and Rothenberg, E. (2017). DNA ligase IV guides end-processing choice during nonhomologous end joining. Cell Rep. *20*, 2810–2819. https://doi.org/10.1016/j.celrep.2017.08.091.

22. Cisneros-Aguirre, M., Lopezcolorado, F.W., Tsai, L.J., Bhargava, R., and Stark, J.M. (2022). The importance of DNAPKcs for blunt DNA end joining is magnified when XLF is weakened. Nat. Commun. *13*, 3662. https://doi.org/10.1038/s41467-022-31365-6.

23. Hammel, M., Yu, Y., Fang, S., Lees-Miller, S.P., and Tainer, J.A. (2010). XLF regulates filament architecture of the XRCC4·ligase IV complex. Structure *18*, 1431–1442. https://doi.org/10.1016/j.str.2010.09.009.

24. Hammel, M., Rey, M., Yu, Y., Mani, R.S., Classen, S., Liu, M., Pique, M.E., Fang, S., Mahaney, B.L., Weinfeld, M., et al. (2011). XRCC4 protein interactions with XRCC4-like factor (XLF) create an extended grooved scaffold for DNA ligation and double strand break repair. J. Biol. Chem. *286*, 32638–32650. https://doi.org/10.1074/jbc.M111.272641.

25. Hammel, M., Yu, Y., Radhakrishnan, S.K., Chokshi, C., Tsai, M.S., Matsumoto, Y., Kuzdovich, M., Remesh, S.G., Fang, S., Tomkinson, A.E., et al. (2016). An intrinsically disordered APLF links Ku, DNA-PKcs, and XRCC4-DNA ligase IV in an extended flexible non-homologous end joining complex. J. Biol. Chem. *291*, 26987–27006. https://doi.org/10.1074/jbc.M116.751867.

26. Kanno, S.I., Kuzuoka, H., Sasao, S., Hong, Z., Lan, L., Nakajima, S., and Yasui, A. (2007). A novel human AP endonuclease with conserved zinc-finger-like motifs involved in DNA strand break responses. EMBO J. *26*, 2094–2103. https://doi.org/10.1038/sj.emboj.7601663.

27. Bekker-Jensen, S., Fugger, K., Danielsen, J.R., Gromova, I., Sehested, M., Celis, J., Bartek, J., Lukas, J., and Mailand, N. (2007). Human Xip1 (C2orf13) is a novel regulator of cellular responses to DNA strand breaks. J. Biol. Chem. *282*, 19638–19643. https://doi.org/10.1074/jbc.C700060200.

28. Iles, N., Rulten, S., El-Khamisy, S.F., and Caldecott, K.W. (2007). APLF (C2orf13) is a novel human protein involved in the cellular response to chromosomal DNA strand breaks. Mol. Cell Biol. *27*, 3793–3803. https://doi.org/10.1128/mcb.02269-06.

29. Macrae, C.J., McCulloch, R.D., Ylanko, J., Durocher, D., and Koch, C.A. (2008). APLF (C2orf13) facilitates nonhomologous end-joining and undergoes ATM-dependent hyperphosphorylation following ionizing radiation. DNA Repair *7*, 292–302. https://doi.org/10.1016/j.dnarep.2007.10.008.

30. Grundy, G.J., Rulten, S.L., Zeng, Z., Arribas-Bosacoma, R., Iles, N., Manley, K., Oliver, A., and Caldecott, K.W. (2013). APLF promotes the assembly and activity of non-homologous end joining protein complexes. EMBO J. *32*, 112–125. https://doi.org/10.1038/emboj.2012.304.

31. Ahel, I., Ahel, D., Matsusaka, T., Clark, A.J., Pines, J., Boulton, S.J., and West, S.C. (2008). Poly(ADP-ribose)-binding zinc finger motifs in DNA repair/checkpoint proteins. Nature *451*, 81–85. https://doi.org/10.1038/nature06420.

32. Rulten, S.L., Cortes-Ledesma, F., Guo, L., Iles, N.J., and Caldecott, K.W. (2008). APLF (C2orf13) is a novel component of poly(ADP-ribose) signaling in mammalian cells. Mol. Cell Biol. *28*, 4620–4628. https://doi.org/10.1128/MCB.02243-07.

33. Corbeski, I., Guo, X., Eckhardt, B.V., Fasci, D., Wiegant, W., Graewert, M.A., Vreeken, K., Wienk, H., Svergun, D.I., Heck, A.J.R., et al. (2022). Chaperoning

of the histone octamer by the acidic domain of DNA repair factor APLF. Sci. Adv. *8*, eabo0517. https://doi.org/10.1126/sciadv.abo0517.

34. Corbeski, I., Dolinar, K., Wienk, H., Boelens, R., and Van Ingen, H. (2018). DNA repair factor APLF acts as a H2A-H2B histone chaperone through binding its DNA interaction surface. Nucleic Acids Res. *46*, 7138–7152. https://doi.org/10.1093/nar/gky507.
35. Wang, D., Zhou, Z., Wu, E., Ouyang, C., Wei, G., Wang, Y., He, D., Cui, Y., Zhang, D., Chen, X., et al. (2020). LRIK interacts with the Ku70–Ku80 heterodimer enhancing the efficiency of NHEJ repair. Cell Death Differ. *27*, 3337–3353. https://doi.org/10.1038/s41418-020-0581-5.
36. Thapar, R., Wang, J.L., Hammel, M., Ye, R., Liang, K., Sun, C., Hnizda, A., Liang, S., Maw, S.S., Lee, L., et al. (2020). Mechanism of efficient double-strand break repair by a long non-coding RNA. Nucleic Acids Res. *48*, 10953–10972. https://doi.org/10.1093/nar/gkaa784.
37. Bergstrand, S., O'Brien, E.M., Coucoravas, C., Hrossova, D., Peirasmaki, D., Schmidli, S., Dhanjal, S., Pederiva, C., Siggens, L., Mortusewicz, O., et al. (2022). Small Cajal body-associated RNA 2 (scaRNA2) regulates DNA repair pathway choice by inhibiting DNA-PK. Nat. Commun. *13*, 1015. https://doi.org/10.1038/s41467-022-28646-5.
38. Unfried, J.P., Marín-Baquero, M., Rivera-Calzada, Á., Razquin, N., Martín-Cuevas, E.M., de Bragança, S., Aicart-Ramos, C., McCoy, C., Prats-Mari, L., Arribas-Bosacoma, R., et al. (2021). Long noncoding RNA NIHCOLE promotes ligation efficiency of DNA double-strand breaks in hepatocellular carcinoma. Cancer Res. *81*, 4910–4925. https://doi.org/10.1158/0008-5472.CAN-21-0463.
39. Waters, C.A., Strande, N.T., Pryor, J.M., Strom, C.N., Mieczkowski, P., Burkhalter, M.D., Oh, S., Qaqish, B.F., Moore, D.T., Hendrickson, E.A., et al. (2014). The fidelity of the ligation step determines how ends are resolved during nonhomologous end joining. Nat. Commun. *5*, 4286. https://doi.org/10.1038/ncomms5286.
40. Wang, J.L., Duboc, C., Wu, Q., Ochi, T., Liang, S., Tsutakawa, S.E., Lees-Miller, S.P., Nadal, M., Tainer, J.A., Blundell, T.L., et al. (2018). Dissection of DNA double-strand-break repair using novel single-molecule forceps. Nat. Struct. Mol. Biol. *25*, 482–487. https://doi.org/10.1038/s41594-018-0065-1.
41. Zhang, Z., Zhu, L., Lin, D., Chen, F., Chen, D.J., and Chen, Y. (2001). The three-dimensional structure of the C-terminal DNA-binding domain of human Ku70. J. Biol. Chem. *276*, 38231–38236. https://doi.org/10.1074/jbc.m105238200.
42. Hu, S., Pluth, J.M., and Cucinotta, F.A. (2012). Putative binding modes of Ku70-SAP domain with double strand DNA: a molecular modeling study. J. Mol. Model. *18*, 2163–2174. https://doi.org/10.1007/s00894-011-1234-x.
43. Costantini, S., Woodbine, L., Andreoli, L., Jeggo, P.A., and Vindigni, A. (2007). Interaction of the Ku heterodimer with the DNA ligase IV/Xrcc4 complex and its regulation by DNA-PK. DNA Repair *6*, 712–722. https://doi.org/10.1016/j.dnarep.2006.12.007.
44. Shirodkar, P., Fenton, A.L., Meng, L., and Koch, C.A. (2013). Identification and functional characterization of a ku-binding motif in aprataxin polynucleotide kinase/phosphatase-like factor (APLF). J. Biol. Chem. *288*, 19604–19613. https://doi.org/10.1074/jbc.M112.440388.
45. Anisenko, A.N., Knyazhanskaya, E.S., Zatsepin, T.S., and Gottikh, M.B. (2017). Human Ku70 protein binds hairpin RNA and double stranded DNA through two different sites. Biochimie *132*, 85–93. https://doi.org/10.1016/j.biochi.2016.11.001.
46. Yoo, S., and Dynan, W.S. (1998). Characterization of the RNA binding properties of Ku protein. Biochemistry *37*, 1336–1343. https://doi.org/10.1021/bi972100w.
47. Oksenych, V., Kumar, V., Liu, X., Guo, C., Schwer, B., Zha, S., and Alt, F.W. (2013). Functional redundancy between the XLF and DNA-PKcs DNA repair factors in V(D)J recombination and nonhomologous DNA end joining. Proc. Natl. Acad. Sci. USA *110*, 2234–2239. https://doi.org/10.1073/pnas.1222573110.
48. Rulten, S.L., Fisher, A.E.O., Robert, I., Zuma, M.C., Rouleau, M., Ju, L., Poirier, G., Reina-San-Martin, B., and Caldecott, K.W. (2011). PARP-3 and APLF function together to accelerate nonhomologous end-joining. Mol. Cell *41*, 33–45. https://doi.org/10.1016/j.molcel.2010.12.006.
49. Chang, H.H.Y., Watanabe, G., Gerodimos, C.A., Ochi, T., Blundell, T.L., Jackson, S.P., and Lieber, M.R. (2016). Different DNA end configurations dictate which NHEJ components are most important for joining efficiency. J. Biol. Chem. *291*, 24377–24389. https://doi.org/10.1074/jbc.M116.752329.
50. Lamm, N., Rogers, S., and Cesare, A.J. (2021). Chromatin mobility and relocation in DNA repair. Trends Cell Biol. *31*, 843–855. https://doi.org/10.1016/j.tcb.2021.06.002.
51. Dyson, H.J., and Wright, P.E. (2005). Intrinsically unstructured proteins and their functions. Nat. Rev. Mol. Cell Biol. *6*, 197–208. https://doi.org/10.1038/nrm1589.
52. Chen, H., Xue, J., Churikov, D., Hass, E.P., Shi, S., Lemon, L.D., Luciano, P., Bertuch, A.A., Zappulla, D.C., Géli, V., et al. (2018). Structural insights into yeast telomerase recruitment to telomeres. Cell *172*, 331–343.e13. https://doi.org/10.1016/j.cell.2017.12.008.
53. Kaczmarski, W., and Khan, S.A. (1993). Lupus autoantigen ku protein binds HIV-1 TAR RNA in vitro. Biochem. Biophys. Res. Commun. *196*, 935–942. https://doi.org/10.1006/bbrc.1993.2339.
54. Luzzietti, N., Brutzer, H., Klaue, D., Schwarz, F.W., Staroske, W., Clausing, S., and Seidel, R. (2011). Efficient preparation of internally modified single-molecule constructs using nicking enzymes. Nucleic Acids Res. *39*, e15. https://doi.org/10.1093/nar/gkq1004.
55. Fili, N., Mashanov, G.I., Toseland, C.P., Batters, C., Wallace, M.I., Yeeles, J.T.P., Dillingham, M.S., Webb, M.R., and Molloy, J.E. (2010). Visualizing helicases unwinding DNA at the single molecule level. Nucleic Acids Res. *38*, 4448–4457. https://doi.org/10.1093/nar/gkq173.
56. Horcas, I., Fernández, R., Gómez-Rodríguez, J.M., Colchero, J., Gómez-Herrero, J., and Baro, A.M. (2007). WSXM: a software for scanning probe microscopy and a tool for nanotechnology. Rev. Sci. Instrum. *78*, 013705. https://doi.org/10.1063/1.2432410.
57. Lee, L., Yu, Y., and Lees-Miller, S.P. (2022). Purification of DNA-dependent protein kinase catalytic subunit (DNA-PKcs) from HeLa cells. Methods Mol. Biol. *2444*, 227–241. https://doi.org/10.1007/978-1-0716-2063-2_14.
58. Kim, R. (2011). Native agarose gel electrophoresis of multiprotein complexes. Cold Spring Harb. Protoc. *2011*, 884–887. https://doi.org/10.1101/pdb.prot4558.
59. Spagnolo, L., Rivera-Calzada, A., Pearl, L.H., and Llorca, O. (2006). Three-dimensional structure of the human DNA-PKcs/Ku70/Ku80 complex assembled on DNA and its implications for DNA DSB repair. Mol. Cell *22*, 511–519. https://doi.org/10.1016/j.molcel.2006.04.013.
60. Strick, T.R., Allemand, J.F., Bensimon, D., and Croquette, V. (1998). Behavior of supercoiled DNA. Biophys. J. *74*, 2016–2028. https://doi.org/10.1016/S0006-3495(98)77908-1.
61. Seidel, R., van Noort, J., van der Scheer, C., Bloom, J.G.P., Dekker, N.H., Dutta, C.F., et al. (2004). Real-time observation of DNA translocation by the type I restriction modification enzyme EcoR124I. Nat. Struct. Mol. Biol. *11*, 838–843. https://doi.org/10.1038/nsmb816.
62. Pastrana, C.L., Carrasco, C., Akhtar, P., Leuba, S.H., Khan, S.A., and Moreno-Herrero, F. (2016). Force and twist dependence of RepC nicking activity on torsionally-constrained DNA molecules. Nucleic Acids Res. *44*, 8885–8896. https://doi.org/10.1093/nar/gkw689.

## STAR★METHODS

### KEY RESOURCES TABLE

| REAGENT or RESOURCE | SOURCE | IDENTIFIER |
|---|---|---|
| Antibodies | | |
| Sheep Polyclonal Digoxigenin Antibody | Bio-Rad | Cat#3210-0488; RRID: AB_620732 |
| Bacterial and virus strains | | |
| Subcloning Efficiency™ DH5α™ Chemically Competent Cells | Thermo Fisher Scientific | Cat#18265017 |
| Chemicals, peptides, and recombinant proteins | | |
| Bovine Serum Albumin (BSA) | New England Biolabs | Cat#B9000S |
| Dithiothreitol (DTT) | Sigma-Aldrich | Cat#43815 |
| ATP | Sigma-Aldrich | Cat#A6559 |
| Biotin | Sigma-Aldrich | Cat#B4501 |
| Dynabeads MyOne™ Streptavidin T1 | ThermoFisher | Cat#65601 |
| Biotin-16-dUTP | Roche | Cat#11093070910 |
| Digoxigenin-11 dUTP | Roche | Cat#11093088910 |
| Deoxynucleoside Triphosphate Set, PCR Grade | Roche | Cat#11969064001 |
| PspOMI Restriction Enzyme | New England Biolabs | Cat#R0653S |
| BsrGI Restriction Enzyme | New England Biolabs | Cat#R0575S |
| Nt.BbvCI Restriction Enzyme | New England Biolabs | Cat#R0632S |
| Tris(2-carboxyethyl)phosphine hydrochloride (TCEP) | Sigma-Aldrich | Cat#C4706 |
| NotI Restriction Enzyme | New England Biolabs | Cat#R0189S |
| XhoI Restriction Enzyme | New England Biolabs | Cat#R0146S |
| HpaI Restriction Enzyme | New England Biolabs | Cat#R0105S |
| Shrimp Alkaline Phosphatase (rSAP) | New England Biolabs | Cat#M0371S |
| T4 DNA Ligase | New England Biolabs | Cat#M0202S |
| DNaseI (RNase free) | New England Biolabs | Cat#M0303S |
| 1 kb DNA Ladder | New England Biolabs | Cat#N3232L |
| Blue/Orange Loading Dye, 6X | Promega | Cat#G18811 |
| UltraPure™ Agarose | Thermo Fisher Scientific | Cat#16500100 |
| TBE Buffer, 10X, Molecular Biology Grade | Promega | Cat#V4251 |
| SYBR® Safe nucleic acid gel stain | Thermo Fisher Scientific | Cat#S33102 |
| cOmplete™ EDTA-free Protease Inhibitor Cocktail | Sigma-Aldrich | Cat#11836170001 |
| TURBO™ DNAse (2U/ul) | Thermo Fisher Scientific | Cat#AM2238 |
| Critical commercial assays | | |
| Superose 6 10/300 GL | Cytiva | Cat#29091596 |
| Strep-Tactin® XT 4 Flow® | IBA | Cat#2-50-12-001 |
| Talon® Metal Affinity Resin | Clontech | Cat#635653 |
| Phusion High-Fidelity PCR Kit | Thermo Fisher Scientific | Cat#F553S |
| GoTaq ® G2 Flexi DNA Polymerase | Promega | Cat#M7805 |
| QIAquick PCR Purification Kit | QIAGEN | Cat#28106 |
| QIAquick Gel extraction Kit | QIAGEN | Cat#28706 |
| QIAprep Spin Miniprep Kit | QIAGEN | Cat#27106 |
| HiScribe™ T7 High Yield RNA Synthesis Kit | New England Biolabs | Cat#E2040S |
| RNA Clean and Concentrator™-100 | Zymo Research | Cat#R1019 |

(*Continued on next page*)

*Continued*

| REAGENT or RESOURCE | SOURCE | IDENTIFIER |
|---|---|---|
| **Deposited data** | | |
| Magnetic Tweezers Data Part 1/2, related to Figures 1, 2, 3 and 4 | This paper; Mendeley Data | Mendeley Data: https://doi.org/10.17632/7wdr63x5h9.1 |
| Magnetic Tweezers Data Part 2/2, related to Figures 5, 6, S4, S5 and S7 | This paper; Mendeley Data | Mendeley Data: https://doi.org/10.17632/4pdz8cv9cz.1 |
| Python code for data analysis | This paper; Moreno-Herrero Lab Github Repository | https://github.com/Moreno-HerreroLab/MTDataProcessing/ |
| **Experimental models: Cell lines** | | |
| Sf9 cells: *Spodoptera frugiperda* cell line derived from strain IPLB-Sf-21-AE | Thermo Fisher Scientific | Cat#11496015 |
| High Five cells: cell line BTI-TN-5B1-4, clonal isolate from *Trichoplusia ni* cell line | Thermo Fisher Scientific | Cat#B85502 |
| **Oligonucleotides** | | |
| DNA oligonucleotides used in this work, see Table S1 | This paper | N/A |
| MT central dsDNA fragment (4292 bp), see Table S2 | This paper | N/A |
| AFM dsDNA fragment (441 bp), see Table S2 | This paper | N/A |
| NIHCOLE lncRNA, see Table S3 for sequence | Unfried et al.[38] | N/A |
| Antisense NIHCOLE RNA, see Table S3 for sequence | This paper | N/A |
| SM2 and SM3 RNAs, see Table S3 for sequences | Unfried et al. 2021[38] | N/A |
| **Recombinant DNA** | | |
| Plasmid: pBluescript II SK+ | Stratagene | Cat#212205 |
| Plasmid; 71dir v3.pBluescript SK + -2 gaps | This paper | N/A |
| Plasmid: pNLrep | Luzzietti et al.[54] | N/A |
| Plasmid: pSP73-JY0 | Fili et al.[55] | N/A |
| Plasmid: pcDNA3.1-NIHCOLE | Unfried et al.[38] | N/A |
| Plasmid: pcDNA3.1-antisense NIHCOLE | This paper | N/A |
| **Software and algorithms** | | |
| SnapGene – Molecular biology software | SnapGene software | www.snapgene.com |
| Python version 3.9 | Python Software Foundation | www.python.org |
| WSxM – AFM processing software | Horcas et al.[56] | www.wsxm.eu |
| **Other** | | |
| DNA sequence analysis | Unidad de Genómica CAI Genómica y Proteómica Facultad CC Biológicas – UCM | https://cai.ucm.es/en/biological-techniques/genomics/ |
| Bio-Rad Gel Doc™ 2000 | Bio-Rad | N/A |
| LabChip GX Touch 24 Nucleic Acid Analyzer | PerkinElmer | Cat#CLS138162 |

## RESOURCE AVAILABILITY

### Lead contact

Further information for resources and requests should be directed to and will be fulfilled by the lead contact, Fernando Moreno-Herrero (fernando.moreno@cnb.csic.es).

### Materials availability

All reagents generated in this study are available from the lead contact without restriction.

### Data and code availability

- Magnetic tweezers raw data have been deposited at Mendeley Data and are publicly available as of the date of publication. DOIs are listed in the key resources table.

- Original code for magnetic tweezers data processing have been deposited at the Moreno-Herrero Lab GitHub repository and is publicly available. Link is listed in the key resources table.
- Any additional information required to reanalyze the data reported in this paper is available from the lead contact upon request.

## EXPERIMENTAL MODEL AND SUBJECT DETAILS

### Insect cells

For the expression of Ku heterodimer, LigaseIV-XRCC4 and XLF, Sf9 cells were grown in suspension using serum-free Sf-900$^{TM}$ II SFM media (Gibco) in 2 L roller bottles at 27°C and 120 rpm and infected at a MOI of 2 once they reached a density of 2 × $10^6$ cells $mL^{-1}$. Cells were harvested after 72 hours by centrifugation at 1000 g.

For APLF, High Five$^{TM}$ cells were grown in suspension using serum-free Sf-900$^{TM}$ II SFM media (Gibco) in 2 L roller bottles at 28°C and 120 rpm and infected at a MOI of 2 once they reached a density of 1.2 × $10^6$ cells $mL^{-1}$. They were harvested after 48 hours by centrifugation at 1000 g.

### Microbe strains

DH5α Competent cells (Subcloning Efficiency$^{TM}$ DH5α$^{TM}$ Chemically Competent Cells, Thermo Fisher Scientific): species E coli, genotype F- Φ80lacZΔM15 Δ(lacZYA-argF) U169 recA1 endA1 hsdR17(rk-, mk+) phoA supE44 thi-1 gyrA96 relA1 λ-. Liquid cultures were grown in LB medium at 37°C with shaking at 170 rpm for 15–18 hours. Cells growing in LB agar plates were grown also at 37°C for 15–18 hours.

## METHOD DETAILS

### NHEJ proteins expression and purification

Ku70-Ku80 was produced by co-expressing full-length Ku80 containing a 10xHis-tag and full-length Ku70 that contains a twin-strep-tag. The tags were placed at the N-terminus in both proteins. Proteins were produced in insect cells using a baculovirus system followed by affinity purification and size exclusion chromatography as described[30] (Figure S2A).

Ku70/Ku80ΔC$^{L68R}$ was expressed and produced similarly as described.[30] Ku80ΔC contains a deletion of the C-terminal domain (deleted amino acids 591–732) that does not affect formation of the Ku ring or binding to dsDNA as described before.[5] Ku70/Ku80ΔC$^{L68R}$ was characterized before and shown to bind DNA *in vitro* and to be recruited to sites of DNA damage in cells[30] (Figure S2B).

The complex between XRCC4 and DNA-Ligase IV was produced by co-expressing both full-length proteins in insect High Five cells. XRCC4 contains a C-terminal 8xHis-tag and DNA-Ligase IV contains an N-terminal twin-strep-tag. Expression and purification were performed as described in detail in the supplementary information of Unfried et al.[38] In brief, cells expressing the complex were lysed and the lysate was clarified by centrifugation using a 0.5 μm filter and loaded on Talon resin (Clontech). The resin was then washed with a buffer supplemented with 5 mM imidazole and eluted in buffer containing 300 mM imidazole. Fractions containing the complex were pooled and loaded onto a Hitrap-Strep column (GE Healthcare). XRCC4-DNA-Ligase IV was eluted with a buffer containing 2.5 mM d-desthiobiotin and the fractions containing the complex were loaded into a 26/60 Superdex 200 column (GE Healthcare) (Figure S2A).

XLF full-length was cloned into pFBDM under the pH promoter, harboring an uncleavable 8xHis C-terminal tag. Protein was expressed using the Multi-Bac baculovirus system, with sf9 cells infected at a density of 2 millions/mL with an MOI of 2. Cells were harvested after 2.5 days, resuspended in 50 mM HEPES pH 7.5, 250 mM NaCl, 10% glycerol, 5 mM TCEP and lysed with a dounce homogeniser. After clarification by centrifugation at 40,000 g for 1 h at 4°C, the supernatant was applied to a Talon-Crude Resin (Cytiva) and protein was eluted by supplementing the previous buffer with 300 mM imidazol. All buffers were supplemented with protease inhibitor tablets (Merck) through-out these initial purification steps. Elution fractions were checked by SDS-PAGE and those containing XLF were pulled together, concentrated and applied to a Superdex 200 16/60 column (Cytiva) pre-equilibrated with 50 mM HEPES, pH 7.5, 200 mM NaCl, 5% glycerol, 5mM TCEP. Peak fractions were checked by SDS-PAGE, concentrated to 10 mg/mL and flash-frozen in liquid nitrogen (Figure S2A).

DNA-PKcs was a kind gift from Dr. Susan P. Lees-Miller at the Department of Biochemistry and Molecular Biology, Robson DNA Science Center, Arnie Charbonneau Cancer Institute, Cumming School of Medicine, University of Calgary, Calgary, Canada. DNA-PKcs was purified as described in Lee et al.[57] (Figure S2C).

Full-length human APLF was expressed in baculovirus harboring an N-terminal twin-strep-tag and a C-terminal 8xHis tag. Insect High Five cells were infected with APLF baculovirus at a MOI of 2 and incubated for 60 h at 26°C. Cells were lysed by homogenization in lysis buffer (50 mM HEPES, pH 8.0, 500 mM NaCl, 10% (w/v) glycerol, 0.5 mM TCEP) supplemented with EDTA-free protease inhibitors (Roche) and TURBO DNase (Life Technologies). After a 20-minute incubation in ice, the slurry was clarified by centrifugation at 50,000 × g for 60 minutes, passed through a 0.5 μm filter and over Talon resin (Clontech) equilibrated with lysis buffer. The resin was then washed with lysis buffer supplemented with 5 mM imidazole and eluted in buffer supplemented with 300 mM imidazole and NaCl to 1M. Fractions containing APLF were identified by SDS-PAGE, pooled, loaded onto a Strep-Tactin-XT cartridge (IBA), and

subsequently eluted with buffer supplemented with 50 mM biotin (Figure S2D). Finally, APLF rich fractions were pooled, concentrated and loaded into a 26/60 Superdex 200 column (Cytiva) equilibrated with storage buffer (50 mM HEPES, pH 8.0, 250 mM NaCl, 10% (w/v) glycerol, 0.5 mM TCEP). Peak fractions from the size exclusion column were aliquoted, flash-frozen, and stored at −80°C. Full-length APLF samples for magnetic tweezers experiments had their twin-strep tag cleaved.

Several mutants of APLF were produced. $APLF^{R27A}$ harbors a mutation in the FHA domain. $APLF^{C387A-C427A}$ contains mutations in both PBZ domains. $APLF^{1-435}$ has a truncation of the C-terminal acidic domain. All these mutants were characterized in Grundy et al.[30] These mutant versions of APLF were expressed and purified as the wild type. Magnetic tweezers experiments using APLF mutants include 1 μM biotin to reduce any potential interaction with the streptavidin-coated beads (Figure S2D).

### Electrophoretic mobility shift assays (EMSAs)

EMSA experiments were performed as described in[58] including some minor modifications. 0.8% agarose gels were prepared in 5X buffer A (1X buffer A corresponds to 25 mM Tris-HCl pH 8.5, 19.2 mM glycine) containing either SYBR® Safe (Invitrogen) or GreenSafe Premium (NZYTech) for DNA or SM3 interaction experiments respectively. Gels were run in 2X buffer A at 50 V and 4°C and visualized using an UV transilluminator at different times ranging from 30 to 150 minutes depending on the experiment. Agarose gels were subsequently stained using Quick Coomassie Stain (NeoBiotech). For the DNA-Ku-X4-LIG4 interaction experiments we used a DNA molecule that has only one accessible end and 60 bp of dsDNA[5,59] (Table S1). SM3 was refolded by temperature treatment ramping as described before prior incubation with the different proteins. In all cases mixtures in stochiometric relationships were incubated for 10 minutes at 4°C, then 2X loading buffer was added and the EMSA experiments performed.[58]

### Bulk ligation of DNA by X4–LIG4

The ligation reactions were conducted as described in Unfried et al.[38] with few modifications. In brief, 40 nM of linear DNA substrate was mixed with 0.1 mg/mL neutravidin (Invitrogen, 22832) for 5 minutes. Then 0.5 mM ATP, 1 mM DTT and 10% PEG-8000, 80 nM Ku70/80, 40 nM X4L4 and 160 nM APLF were added. The reaction was incubated at 37°C for 90 minutes and DNA was extracted with phenol-chloroform (Sigma, 77617) and precipitated with ethanol. Ligation products were resolved in a 15% native PAGE in 1x TBE, DNA was stained with a 1/10,000 solution of SYBR safe (Invitrogen, S33102) in 1x TBE for 15 minutes and visualized using a Chemidoc MP instrument. Quantitation of ligation product was performed using the ImageLab software (Bio-Rad).

### AFM experiments with Ku and APLF

Atomic Force Microscopy (AFM) samples were prepared by depositing 20 μL of sample in 20 mM HEPES-KOH pH 7.8 buffer for 10 min onto a mica pretreated with 30 mM spermidine for another 10 min. After adsorption, samples were cleaned with 3 mL of Milli-Q water and dried with nitrogen or argon gas. For these experiments, a blunt dsDNA fragment (441 bp) was obtained by digestion of a homemade plasmid with HpaI followed by gel extraction and purification (QIAGEN). DNA-only samples were prepared for a final concentration of 0.5 nM. All samples containing proteins were prepared for final concentrations of 0.4 nM DNA, 10 nM Ku, and 20 nM APLF. In samples containing DNA and Ku, both components were incubated at room temperature for 5 min prior deposition. In samples containing APLF, DNA and Ku, DNA and Ku were firstly incubated for 5 min following addition of APLF and incubation for additional 5 min prior deposition. Images were obtained in tapping mode in air, using an AFM from Nanotech Electronica S. L. with PointProbePlus tips (PPP-NCH Nanosensors). Image processing consisted of flattening and plane subtraction using WSxM software.[56]

### Magnetic tweezers DNA substrates

The branched dsDNA constructs for magnetic tweezers (MT) consist of a central dsDNA fragment of 4292 bp with two centric 60-bp branches separated by 689 bp. Branches were customized to end in blunt or cohesive (4-nt 5′-overhangs) terminations depending on the assay. The central fragment was flanked by two highly labeled DNA handles, one with digoxigenins and the other with biotins, of 1 kbp and 140 bp, respectively. Biotinylated handle was shorter to avoid the attachment of two beads per DNA tether. DNA oligonucleotides used to fabricate the MT DNA substrates are included in Table S1. The sequence of the central part of the MT substrates is included in Table S2.

The central part of the MT DNA substrate is based on the plasmid 71dir v3.pBluescript SK + -2 gaps (4307 bp). The plasmid contains two regions of five spaced BbvCI restriction sites with the same orientation. To produce this plasmid, a poly-BbvCI region was extracted from the pNLrep plasmid (kindly gifted by Prof. Dr. Ralf Seidel) and cloned twice into a modified pBluescriptIISK + plasmid (Stratagene). Plasmids were cloned in DH5α Competent cells (Thermo Fisher Scientific) and potential positive colonies were then selected by colony PCR. Plasmids were purified from cultures using QIAprep Spin Miniprep Kit (QIAGEN), analyzed by digestion with restriction enzymes, and finally checked by DNA sequence analysis. The central part of the MT construct was obtained by digesting the plasmid 71dir v3.pBluescript SK + -2 gaps (4307 bp) with PspOMI and BsrGI enzymes followed by purification (QIAGEN). The 4292 pb product (Table S2) was then digested with Nt.BbvCI (New England Biolabs). This produced two sets of five nicks on one of the strands leading to two 63 nt gaps during heat inactivation of the nicking enzyme.[54] Branches were produced by annealing two partially complementary oligonucleotides (Table S1) by heating at 95°C for 5 minutes and cooling down to 20°C at a $-1°C\ minute^{-1}$ rate in hybridization buffer (10 mM Tris-HCl pH 8.0, 1 mM EDTA, 200 mM NaCl, 5 mM $MgCl_2$). Branches contain a 60-bp duplex stem ending either in a blunt end or cohesive end (4 nt overhang) and two single-stranded regions complementary to the gaps created by

Nt.BbvCI (Figure S1). A 150X excess of branches was annealed into the created gaps by heating 5 min at 80°C, and slowly cooling down to 30 °C at a 0.5 °C $min^{-1}$ rate in annealing buffer (50 mM Tris-HCl pH 8.0, 1 mM EDTA, 100 mM NaCl). Handles were prepared by PCR (see Table S1 for primers) including 200 μM final concentration of each dNTP (G, C, A), 140 μM dTTP and 66 μM Bio-16-dUTP or Dig-11 dUTP (Roche) using plasmid pSP73-JY0 [59] as template, followed by digestion with the restriction enzyme BsrGI or PspOMI respectively. Dig-labelled handle was dephosphorylated with rSAP (New England Biolabs) to ensure relaxed tethers. Labeled handles were ligated with the central part overnight with T4 DNA Ligase (New England Biolabs). Sample was then ready to use in MT experiments without further purification. DNAs were never exposed to intercalating dyes or UV radiation during their production and were stored at 4°C.

An unbranched dsDNA construction was prepared in a similar way but omitting the steps of digestion of the central part with Nt.BbvCI. The purified central DNA fragment was directly ligated with the handles.

To fabricate the construct with cohesive branches the order of the steps is slightly different to avoid the self-ligation of the cohesive ends of the branches during the last step of ligation. This specific construct was prepared over the unbranched dsDNA construct, which already has ligated handles. The unbranched substrate was digested with Nt.BbvCI and after inactivation of the enzyme, a 150X excess of branches with cohesive ends was annealed into the created gaps as described above. The substrate was ready to use without any additional step of ligation that would seal the nicks present. This construct was only used in the T4 ligation assay.

### DNA plasmids for RNA *in vitro* transcription

The cloning of NIHCOLE into pcDNA3.1 for *in vitro* transcription was previously described.[38] For antisense insertion of the sequence of NIHCOLE into pcDNA3.1, the original plasmid pcDNA3.1-NIHCOLE was used as template for PCR amplification of NIHCOLE sequence (see Table S1 for primers). The PCR fragment was digested with NotI and XhoI and ligated into the previously purified vector pcDNA3.1 obtained by digestion of pCDNA3.1-NIHCOLE with NotI and XhoI followed by gel extraction (QIAGEN). The plasmid was cloned, analyzed, and sequenced as described above.

### RNA *in vitro* transcription

NIHCOLE and asNIHCOLE RNAs were synthesized by *in vitro* transcription reaction. For *in vitro* transcription, NIHCOLE and asNIHCOLE templates were prepared by PCR amplification with Phusion High-Fidelity DNA Polymerase (Thermo Scientific) using forward primers with a T7 promoter adapter (see Table S1 for primers) followed by purification (QIAGEN). Purified templates were transcribed using the HiScribe T7 High Yield RNA Synthesis Kit (New England Biolabs) following the manufacturer's instructions with minor modifications.[38] Reactions were assembled in 10 μL final volume containing 500 ng of DNA template and incubated for 10 h at 37°C. Transcription products were treated for 1 h at 37°C with 2.5 units of RNase-free DNase I (New England Biolabs) to remove the DNA template. The RNA was then cleaned up with RNA Clean and Concentrator-100 columns (ZymoResearch) but eluted with 5 mM Tris-HCl pH 8.5. After that, RNAs were refolded by temperature treatment ramping down from 65°C (10 min) to 4°C (1°C decrease every 40 s) as described in Unfried et al.[38] RNA concentration was determined using a NanoDrop spectrophotometer. Size and integrity of RNAs were assayed by automated RNA electrophoresis in a LabChip GX Touch 24 Nucleic Acid Analyzer (PerkinElmer). RNA samples were aliquoted and stored at −80°C. See Table S3 for RNA sequences. DNA templates for SM2 and SM3 and RNA transcription were obtained as described in Unfried et al.[38]

### Magnetic tweezers setup

Magnetic tweezers assays were performed in a custom-built setup like previously described.[60–62] Briefly, the equipment consists of a microfluidic chamber arranged on top of an inverted microscope. The microscope is equipped with a high magnification oil-immersion objective and connected to a CCD camera. A pair of vertically aligned magnets located above the microfluidic chamber allowed us to apply forces to superparamagnetic micrometer size beads tethered to the lower glass surface of the fluid chamber by DNA molecules. The motion of the magnetic beads was recorded at 120 Hz and the XYZ spatial coordinates were extracted from the images obtained with CCD camera with nanometer resolution. In our setup, forces up to 5 pN can be applied to 1 μm beads and up to 30–40 molecules can be tracked simultaneously at 120 Hz.

### DNA incubation and immobilization

4 μL of DNA stock (1.14 nM) diluted 1:300 in TE (10 mM Tris, 1 mM EDTA, pH 8.0) was mixed with 10 μL of commercial beads (Dynabeads MyOne Streptavidin T1) diluted 1:10 in in phosphate buffered saline buffer (PBS) with 0.4 mg/mL BSA (New England Biolabs). The mix was incubated for 10 min while re-suspending occasionally. At this point, the biotinylated handle of the DNA construction attached to the streptavidin functionalized beads. Next, the excess of DNA in solution was removed by trapping the beads with a magnet, discarding all the volume, and re-suspending the pellet again. This cleaning step was repeated three times. The functionalized beads were finally re-suspended in PBS with 0.4 mg/mL BSA to a final volume of 80 μL and flushed into the microfluidic chamber. Once inside the chamber, the digoxigenin-labelled handle immobilized the DNA molecules to the lower glass surface covered in anti-digoxigenin. After 15 min, the excess of beads was washed away by flushing PBS. The incubation process can be repeated several times to obtain the desired number of molecules per field of view.

### In-chamber T4 ligation assay

For the ligation assay with T4 DNA Ligase in the MT the branches of the DNA construction must have cohesive ends to increase the probability of ligation. The DNA was tethered inside the chamber as described in the previous section. Then, the buffer inside the chamber was exchanged to the T4 DNA Ligase Buffer (New England Biolabs). The molecules of interest were tested to rule out the beads bound to more than one DNA molecule. While maintaining a force of 2 pN the enzyme was added to the chamber. 2 μL of T4 DNA Ligase (New England Biolabs) in 98 μL of T4 DNA Ligase buffer. Once the enzyme was inside the chamber the molecules were relaxed by reducing the force to 0.1 pN for 30 min. After that time the force was returned to 2 pN. If the ligation was successful, the branches would be ligated forming a bridge, which translates into a reduction in extension.

### In-chamber force cycles assay

For the study of synaptic events a sequence of force cycles was programmed and applied for all the conditions studied. The sequence was the following: a starting step of 2 min at a higher force (2 pN), followed by a 10 s step at the same force (2 pN) to define the initial extension of each molecule and then 40 repetitions of a two steps cycle, being the first step 10 s at a lower force (0.1 pN) and the second step 10 s at a higher force (2 pN). To start a force cycles assay, the DNA was first tethered inside the chamber as described in a previous section. Once a good number of tethers was achieved the proteins and/or RNA were flushed into the chamber and incubated for 5 min. Then, for each new area of tracking the molecules of interest were tested to rule out beads bound to more than one DNA molecule. Next, the force sequence was applied. All assays were conducted in 20 mM Hepes-KOH (pH 7.8), 100 mM KCl, 5 mM $MgCl_2$, 1 mM DTT and 0.5 mg/mL BSA. X4-LIG4, APLF, lncRNA NIHCOLE, asNIHCOLE, SM2 and SM3 fragments, when present, were used at a concentration of 10 nM. XLF, when present, was used at a concentration of 5nM and Ku70-Ku80, when present, was added at a concentration of 1 nM.

## QUANTIFICATION AND STATISTICAL ANALYSIS

Datasets obtained from the MT assays were analyzed using original Python scripts. A representative example of the analysis workflow can be found at the Moreno-Herrero Lab GitHub repository, the link is listed in key resources table. The output parameter obtained from the MT assays is the absolute extension for each molecule with respect to time and applied force. These absolute extensions differ from one molecule to the other, due to variabilities in the attachment points. To reduce the impact of this variability all individual absolute extensions were transformed into relative extensions taking as a reference point the averaged initial extension of each molecule. The resulting parameter, $\Delta z$, is the reduction in extension with respect to the initial value. $\Delta z$ is 0 μm if the molecule maintains its initial extension and is <0 μm if the extension is reduced. To obtain the extension distributions, for each condition studied, the relative extensions obtained from the different molecules and the different replicates were merged into a single dataset and processed to obtain a histogram of the merged frequency for each relative extension. The distributions were normalized so that the area under the curve is 1. Gaussian fittings to the extended and synaptic peaks were obtained by fitting the $\Delta z$ data within the intervals [-0.05 μm, +0.05 μm] and [-0.25 μm, −0.15 μm], respectively. The peak maxima are marked at the respective $\Delta z$ positions and the percentages marked within the peak (both included in Figures 1, 2, 3, 4, 5 and 6) indicate the weight of each peak to the total number of points. To estimate the errors associated to synaptic probabilities, we randomly select a sampling set of 100 beads, from which we compute a probability density, and from the Gaussian fitting, a synaptic probability. This procedure is repeated 50 times to calculate an average synaptic probability and its standard deviation (shown as errors in Figures 1, 2, 3, 4, 5 and 6). The population size of each distribution, corresponding to the number of molecules tracked and processed for each condition, was marked in Figures 1, 2, 3, 4, 5 and 6 as an N in the lower left corner of each $\Delta z$ density plot. To extract the dwell times ($\tau$), defined as the time since the pulling starts until the DNA-bridge ruptures, the individual traces of the molecules were first fragmented into individual cycles and then smoothed out with a moving average (rolling window of 10 frames). The extension at each point was evaluated, and the first point with an extension within the interval [-0.05 μm, +0.05 μm] was taken as the rupture moment. For each molecule we obtained 40 $\tau$ values, one per cycle, and from all the $\tau$ values obtained per condition we computed an average dwell time. The violin plots in Figures 1, 2, 3, 4, 5 and 6 represent the $\tau$ distributions for the conditions mentioned in the respective Figure. The densities of the violin plots were normalized to the width, and the averaged dwell times were marked in the respective $\tau$ position by dark circles.